BIODEGRADABLE SILICON-CONTAINING ELASTOMERS FOR TISSUE ENGINEERING SCAFFOLDS AND SHAPE MEMORY POLYMERS

A Thesis

by

CODY A. SCHOENER

Submitted to the Office of Graduate Studies of
Texas A&M University
in partial fulfillment of the requirements for the degree of

MASTER OF SCIENCE

August 2009

Major Subject: Biomedical Engineering

BIODEGRADABLE SILICON-CONTAINING ELASTOMERS FOR TISSUE ENGINEERING SCAFFOLDS AND SHAPE MEMORY POLYMERS

A Thesis

by

CODY A. SCHOENER

Submitted to the Office of Graduate Studies of
Texas A&M University
in partial fulfillment of the requirements for the degree of

MASTER OF SCIENCE

Approved by:

Chair of Committee,	Melissa A. Grunlan
Committee Members,	Mariah Hahn
	Elizabeth Cosgriff-Hernandez
Head of Department,	Gerard L. Cote

August 2009

Major Subject: Biomedical Engineering

ABSTRACT

Biodegradable Silicon-Containing Elastomers for Tissue Engineering Scaffolds and Shape Memory Polymers. (August 2009)

Cody A. Schoener, B.S., Texas A & M University

Chair of Advisory Committee: Dr. Melissa A. Grunlan

Commonly used thermoplastic biodegradable polymers are generally brittle and lack appreciable elasticity at physiological temperature and thereby fail to mimic the elastic nature of many human soft tissues such as blood vessels. Thus, there is a need for biomaterials which exhibit elasticity. Biodegradable elastomers are promising candidates whose elasticity more closely parallels that of soft tissues. In this research, we developed hybrid biodegradable elastomers comprised of organic and inorganic polymer components in a block copolymer system: poly(ε-caprolactone) (PCL) and poly(dimethylsiloxane) (PDMS), respectively. A block structure maintains the distinct properties of the PCL and PDMS components. These elastomers may be useful for the tissue engineering of soft tissues as well as for shape memory polymer (SMP) devices.

Tri-block macromers of the form PCL_n-*block*-$PDMS_m$-*block*-PCL_n were developed to permit systematic variations to key features including: PDMS block length, PCL block length, PDMS:PCL ratio, and crosslink density. The macromer was capped with acrylating groups (AcO) to permit their photochemical cure to form elastomers. Thus, a series of biodegradable elastomers were prepared by photocrosslinking a series

of macromers in which the PCL blocks varied (n = 5, 10, 20, 30, and 40) and the PDMS block was maintained (m = 37). All elastomers displayed hydrophobic surface properties and high thermal stability. These elastomers demonstrated systematic tuning of mechanical properties as a function of PCL block length or crosslink density. Notable was strains at break as high as 814% making them suitable for elastomeric bioapplications.

Elastomers with a critical PCL block length (n = 30 or 40) exhibited shape memory properties. Shape memory polymers based on an organic-inorganic, photocurable silicon-containing polymer system is a first of its kind. This SMP demonstrated strain fixity of 100% and strain recovery near 100% after the third thermomechanical cycle. Transition from temporary to permanent shape was quite rapid (2 sec) and at temperatures near body temperature (60 °C). Lastly, porous analogues of the biodegradable elastomers were created using a novel porogen – salt leaching technique. Resulting porous elastomers were designed for tissue engineering scaffolds or shape memory foams.

DEDICATION

To my wife, Molly Marie Schoener, and baby boy, Noah Reinhart Schoener. Both were vital to the completion of this research by providing the necessary support, patience, and love throughout the completion of my degree.

ACKNOWLEDGEMENTS

I would like to thank my research advisor, Professor Melissa A. Grunlan, who initially sparked my interest in polymer science and ability to develop next generation materials for bioapplications. Through her guidance, I am now a research scientist who can think, analyze, and solve problems. Furthermore, I can complete research in a controlled, systematic manner resulting in data that is meaningful and publishable.

I would also like to thank my committee members, Professor Mariah Hahn and Professor Elizabeth Cosgriff-Hernandez, for their shared wisdom on specific subject areas as well as use of laboratory equipment and space.

Thanks also go to my friends and colleagues and the department faculty and staff for making my time at Texas A&M University a great experience. I also want to extend my gratitude to the National Science Foundation GK-12 Program and Dr. Eric Simanek, for the financial support and opportunity to work with academically disadvantaged elementary students.

Finally, thank you to my mother and father for sacrifices taken to send me to Texas A & M University and continual support through life.

TABLE OF CONTENTS

CHAPTER Page

LIST OF FIGURES

FIGURE Page

LIST OF TABLES

CHAPTER I

INTRODUCTION

1.1 Overview

Biomaterials are materials that can function as a whole or part of a device to treat, assist, repair, or replace any tissue, organ, or function of the body. Biodegradability, mechanical properties, and ease of fabrication of a biomaterial are critical factors in determining feasibility and long-term success. Biodegradability eliminates the need for subsequent surgical interventions to remove an implant and eliminates problems associated with long-term implant tolerance. In tissue engineering, biodegradable polymer scaffolds degrade allowing the space which they occupied to be replaced by regenerated tissue. For biomaterials, both the rate and the biodegradation mechanism (i.e. homogeneous versus heterogeneous) must be considered because of its impact on mechanical properties. In certain applications, particularly those involving soft tissue treatment or regeneration, a biomaterial which can exhibit large, cyclical deformations is desirable. In addition, biomaterials which are able to also dramatically change their shape after an increase in temperature (i.e. shape memory) may permit minimally invasive surgical procedures. Thus, biodegradable elastomers, particularly those which are thermosets formed by rapid photochemical cure, are promising candidates where homogeneous biodegradation, elasticity, ease of fabrication, and even shape memory behavior are required.

This thesis follows the style of *Journal of American Chemical Society*.

1.2 Introduction

Tissues or organs may become too diseased or injured to repair themselves naturally. Thus, the invention and implantation of a biomaterial serving a temporary replacement, support, or fixation role is necessary.[1] Biodegradable polymers are a class of biomaterials which can serve these functions. Hydrolytic, enzymatic, and/or oxidative cleavage reduces biodegradable polymers to monomeric or oligomeric forms which are then excreted from the body. Biodegradable polymers are advantageous because they eliminate the need for a second surgical intervention for removal.[2] Some medical devices composed of biodegradable polymers are commercially available (Table 1.1). Unfortunately, conventional thermoplastic biodegradable polymers such as poly(glycolic acid) (PGA) and poly(lactic acid) (PLA) are generally brittle and lack appreciable elasticity at physiological temperatures (Table 1.2). The lack of elasticity of many amorphous or semi-crystalline thermoplastic biodegradable polymers is attributed to a glass transition temperature (T_g) above physiological temperature and is further diminished with increased levels of crystallinity. Hence, these polymers fail to mimic the elastic nature of many soft tissues such as blood vessels, cartilage, and ligaments.[3] Thus, biodegradable elastomers are a unique biomaterial for medical applications because they exhibit highly elastic characteristics at physiological temperatures. The chemical composition and crosslink density of biodegradable elastomers may be tailored such that they are capable of exhibiting tunable physical properties, including: degradation, mechanical, thermal, and surface properties. A biodegradable elastomer with a T_g below body temperature (37 °C) will permit it to more closely parallel the elastic nature of soft

tissues (Table 1.2). Like biodegradable polymers, biodegradable elastomers also degrade via hydrolysis into oligomers and compounds capable of being elmininated by the human body. Biodegradable elastomers may be prepared as thermoplastics[4-8] through solvent casting or as thermosets[9-12] crosslinked via heat or ultraviolet (UV) light. Finally, through chemical synthesis and post-synthesis fabrication, biodegradable elastomers can be targeted for soft tissue engineering (TE) scaffold and shape memory polymer applications.

Table 1.1. Commercially available biodegradable medical devices[2]

Device	Composition	Trade Name	Manufacturer
Suture	PGA	Dexon	Davis and Geck
	PGA-PLLA	Vicryl	Ethicon
	PGA-PCL	Monocryl	Ethicon
	PDO	PDS	Ethicon
	PGA-PLLA	Polysorb	U.S. Surgical
	PGA	PGA Suture	Lukens
Interference Screws	PDLLA	Sysorb	Synos
	PLLA	Arthrex	Arthrex
	PLLA	Bioscrew	Linvatec
	PLLA-PDLLA	Phusiline	Phusis
	PGA-PDLLA	Biologically Quiet	Instrument Makar
Suture Anchor	PLLA	Bio-Statak	Zimmer

Table 1.2. Common biodegradable polymer properties

Polymer	Glass-Transition Temperature (T_g, °C)	Melting Temperature (T_m, °C)	Degradation Time (months)
Poly(L-lactic acid)	60 – 65	173 – 178	>24
P(D,L-lactic acid)	55 – 60	Amorphous	12 – 16
Poly(glycolic acid)	35 – 40	225 – 230	6 – 12
Poly(ε-caprolactone)	(-65) – (-60)	43 – 60	>24
Poly(dioxanone)	(-10) – 0	--	6 – 12

Critical factors in the design of biomaterials include mechanical properties, biodegradability, and ease of fabrication. Many biomaterials, when in implanted, are subjected to forces or loads. For example, a tissue engineered artery would experience pulsatile blood flow.[13] On the other hand, TE knee meniscus would experience compression for shock absorption during walking or running.[14] Therefore, it is necessary to design biomaterials with mechanical properties which mimic those of the tissue or organ that is it replacing or assisting. The mechanical behavior of a material reflects the relationship between its response or deformation to an applied load or force.[15] Important mechanical properties are those tested in tension including tensile strength, tensile modulus, and percent elongation. Tensile strength is the maximum stress a biomaterial will sustain when in tension, beyond this, fracture and failure of the biomaterial will result. Tensile modulus, also known as Young's Modulus, indicates a biomaterials resistance to elastic deformation and reflects its stiffness or rigidity. Elastic deformation is nonpermanent and recoverable when the applied load is released. Percent elongation is a measure of the degree of deformation that is sustained before biomaterial fracture. Force may also be applied in compression, shear, and torsion.

Conventional thermoplastic biodegradable polymers such as PLA and PGA are more rigid and lack the elasticity of many soft tissues (Table 1.3). On the other hand, biodegradable elastomers are capable of large, recoverable deformation. Biodegradable elastomer mechanical properties can be modulated through synthesis of di-, tri-, or multi-polymers, architecturally arranged in block, star, or linear structures, and prepared as thermoplastics or thermosets. Biodegradable thermoplastics reported in the literature

include: poly(ester-urethane)s[16-20] and polyesters such as poly(diol citrates),[21-25] poly(glycolide-*co*-caprolactone),[26] and poly(4-hydroxybutyrate)s.[27, 28] Biodegradable thermosetting elastomers have been prepared by chemically crosslinking poly(lactone)s,[29] poly(ε-caprolactone)s,[30, 31] polyphosphazenes,[32, 33] poly(glycerol-sebacate),[34, 35] and *star*-poly(ε-caprolactone-*co*-D,L-lactide).[36, 37] Biodegradable elastomers have traditionally been composed of PCL or PDO and copolymerized with PGA or PLA's. However, a new set of biodegradable elastomers are emmerging such as poly(glycerol sebacate) and poly(diol citrates). Poly(glycerol sebacate) combine glycerol and sebacic acid to form biocompatible, biodegradable polymers that are easy to synthesize and alter mechanical properties.[38] Glycerol is the basic building blocks for lipids and sebacic acid plays an intermediate role in oxidation of fatty acids.[39] Poly(diol citrates) are based on linear aliphatic diols or polyether diols polymerized with citric acid.[40] Citric acid is a metabolic product of the body (Krebs or citric acid cycle) and non-toxic.

Table 1.3. Human soft tissue[41-45] and biodegradable polymer[46, 47] mechanical properties

Tissue	Modulus (MPa)	Tensile Strength (MPa)	Strain at Break (%)
Smooth Muscle, relaxed	0.006	-	300
Smooth Muscle, contracted	0.01	-	300
Carotid Artery	.084 +/- .022	-	-
Pericardium	20.4 +/- 1.9	-	34.9 +/- 1.1
Cerebral Artery	15.69	4.34	50
Cerebral Vein	6.85	2.82	83
Patellar Tendon (29-50 yrs. old)	660 +/- 266	64.7 +/- 15	14.0 +/- 6.0
Ligaments: ACL, PCL, LCL (21-30 yrs. old)	345 +/- 22.4	36.4 +/- 2.5	15.0 +/- 0.8
Polymer			
Poly(glycolid acid)	6900	70	15 - 20
Poly(L-lactic acid)	2800 - 4200	28 - 50	6
Poly(D,L-lactic acid)	1400 - 2800	27.6 - 41.4	3 - 10
Poly(ϵ-caprolactone)	400	16	16

The manner in which biodegradable materials degrade is also of importance. If a biomaterials mechanical integrity fails before a significant amount of mass loss during biodegradation, the implant will fail. Degradation can be either heterogeneous or homogenous. Heterogeneously degradation occurs because amorphous regions degrade more quickly (due to greater water penetration) than the crystalline domains.[29] Semi-crystalline thermoplastics composed of biodegradable polymers may exhibit heterogeneous degradation.[48] On the other hand, thermosets may help control degradation profiles through crosslink density, hydrophilicity, and in some cases, the degree of crystallinity.

Biodegradable elastomers can be synthesized of one or many biodegradable polymers which can control mechanical properties and biodegradation rates. For

example thermoplastic PCL and PDLLA degrade in 24 and 12 – 16 months, respectively. To decrease degradation time, thermoset elastomers of PCL:PDLLA have been developed in ratios of 30/70, 50/50, and 70/30 resulting in 30%, 25%, and 10% mass loss over 12 wks, respectively.[12] Furthermore, mechanical properties of these ranged from 0.64 – 5.2 MPa Young's modulus, 1.0 – 9.7 MPa tensile strength, and 100 – 190% strain at break. Similar manipulation of mechanical properties and degradation rates of copolymer compositions has been reported.[4, 49, 50]

Polymer architecture can influence biodegradable elastomers properties. Architecture is highly variable, but block and star copolymer systems are popular for elastomer preparation.[36, 37, 51] Block copolymers demonstrate a unique ability to self-assemble into periodic nanostructures producing materials with a broad range of amphiphilic characteristics and unique surface properties.[52] Biodegradable block copolymers are of increasing interest to tailor degradation properties, mechanical properties, and even biocompatibility of the component polymers.[53, 54]Star copolymers can increase crosslink density and further extend mechanical properties.

Porosity is an important consideration for biomaterial applications. For tissue engineering, polymers should be highly porous and interconnected ensuring a high surface area for cell growth and attachment, tissue in growth, and the diffusion of nutrients and cellular waste products.[55] Porosity size and percent porosity of an elastomers system can be customized to optimize attachment and growth for specific cell types: 20 μm (for the in growth of fibroblasts and hepatocytes), 20-150 μm (for skin regeneration), and 100-250 μm (for bone regeneration).[56-58] A variety of methods have

been reported to prepare porous polymeric materials including phase separation, gas foaming, emulsion freeze-drying, rapid prototyping techniques, and solvent-casting and salt leaching.[59-62] Porosity can also increase degradation rate by increasing percent porosity or increasing pore size resulting in increased surface area in contact with degrading media.[63, 64]

Biodegradable elastomers are unique systems which provide elastic properties and biodegradation making them suitable materials for bioapplications. With the development of new biodegradable elastomers in conjunction with improved or novel synthesis and fabrication techniques, mechanical properties and degradation rates can be systematically controlled. In this way, elastomers can be synthesized with properties that closely parallel the tissue of interest.

In this thesis, photosensitive macromers composed of poly(ε-caprolactone) (PCL) and poly(dimethylsiloxane) (PDMS) were crosslinked into thermoset, biodegradable elastomers. The macromer structure and PCL content were related to physical properties including mechanical, thermal, and surface properties. These findings will enable the rational design of future biodegradable elastomers for TE scaffolds or shape memory polymers.

CHAPTER II

BIODEGRADBLE SILICON-CONTAINING ELASTOMERS

2.1 Introduction

Elastomeric biomaterials are useful to treat, repair, or replace damaged or diseased soft tissues as they are capable of large and reversible cyclic deformations without failure. They may also minimize irritation to neighboring soft tissues[34] and reduce fibrous encapsulation of the implant.[65] Biodegradable elastomers would exhibit advantageous degradation profiles compared to thermoplastic polymers. As amorphous thermosets, they would be expected to exhibit homogeneous degradation and linear loss in mechanical properties prior to substantial mass loss.[66] Biodegradable elastomers would be particularly useful in tissue engineering and for minimally invasive, short-term implanted devices. In tissue engineering (TE), biodegradable elastomeric scaffolds would initially exhibit the elasticity of soft tissues, but upon degradation would allow the space which they occupied to be replaced by regenerated tissue. In addition, elastomeric biomaterials may be designed to exhibit a shape-memory such that they are able to dramatically change their shape after an increase in temperature. This may permit minimally invasive surgical procedures involving implantation of bulky devices (e.g. a self-expanding stent). Furthermore, a biodegradable shape memory elastomer would eliminate the need for subsequent surgical removal of the implant and reduce complications associated with long-term implants.

TE seeks to replace damaged or diseased tissues with new healthy tissues.[67] Biodegradable polymer scaffolds provide a 3-D environment in which living cells can attach, differentiate, and produce extracellular matrix (ECM) and hence new tissues.[68-70] There is a current need for scaffolds capable of undergoing long-term cyclic strain without losing mechanical properties for tissue engineering of soft tissues. Biodegradable elastomers are a class of biomaterials capable of withstanding cyclic strain, providing a surface compatible with cell attachment and growth, and degrading at a slow rate allowing load to transfer from scaffold to new tissue.[71] State of the art elastomer TE scaffolds are focusing on novel copolymerization of degrading polymers and unique fabrication techniques to achieve specific mechanical properties. One such system is a scaffold based on microporous poly(L-lactide-co-ε-caprolactone) for articular cartilage tissue engineering.[72] By incorporating micropores, the scaffold can temporarily deform upon loading with little structural collapse and recover to the original geometry upon unloading. A second system developed a biodegradable tubular scaffold for small diameter blood vessel engineering. This novel method coated a porous layer of PCL on the outside of a poly(glycolic-co-lactic acid) fiber braided tube.[73] The porous PCL coating encourages cell attachment and proliferation while the braided fiber provides structural support and inner diameter control of resulting tissue engineered blood vessel. A biodegradable elastomeric scaffold whose physical properties may be systematically altered would be quite useful to establish predictive relationships to end point engineered tissue mechanical properties.

Shape memory materials are stimuli-responsive materials having the capability of changing their shape upon application of an external stimulus (e.g. heat or light).[74, 75] Unlike metal and ceramic counterparts, shape memory polymers (SMPs) are easy to form, light in weight, exhibit large recoverable deformation, and show good processing performance.[76] Therefore, SMPs are being considered for utilization in areas traditional polymers have existed such as the packaging, auto, and textile industries. However, special interest and research expansion is taking root in the biomedical field. An SMPs ability to transform into a temporary deformed shape has led to an explosion in minimally invasive biomedical applications including smart sutures,[77] vascular stents,[78, 79] and microfluidic devices.[80, 81] SMPs can improve patient recovery time and health because they can be fabricated from biocompatible, biodegradable materials which eliminate subsequent surgeries as well as reduce host response as compared to metal or other non-polymer implants.

SMPs consist of "switching segments" and "netpoints" which work cooperatively to achieve the shape memory effect. The netpoints determine the permanent shape and may be either chemical or physical crosslinks. The switching segments exhibit a thermal transition temperature (T_{trans}). Thus, a temporary shape formed by the application of stress at $T > T_{trans}$ is fixed by cooling the deformed SMP at $T < T_{trans}$ and the permanent shape subsequently recovered by reheating to $T > T_{trans}$. Thus, upon heating to $T > T_{trans}$, chain mobility of the switching segments is enhanced to permit shape recovery. T_{trans} can either be the melting temperature (T_m) or glass transition temperature (T_g).[82-84] The shape memory effect through a T_m is relatively quicker and over a narrow temperature range

compared to a T_g. The netpoints must be thermally stable at $T > T_{trans}$ to ensure the conservation of the permanent shape.

SMPs are characterized by three main features which may determine their utility and efficacy: T_{trans}, strain fixity, and strain recovery. For biomedical applications, the value of T_{trans} of an SMP is of critical importance. A T_{trans} near or slightly greater than body temperature (37 °C) would permit shape recovery upon implantation and is acceptable if the amount and duration of external heat applied to induce shape recovery is within the limits of that tolerated by the surrounding tissue. A T_{trans} equal to body temperature could result in premature device deployment during implantation. Strain fixity quantifies the ability of an SMP's to maintain or fixate its temporary shape at $T < T_{trans}$ and strain recovery quantifies its ability to recover the permanent shape at $T > T_{trans}$. A limitation of physically crosslinked SMPs is their insufficient shape fixity and recovery which is manifested as creep and irreversible deformation.[74]

Biodegradable SMPs based on both physically and chemically crosslinked poly(ε-caprolactone) (PCL) has received much attention due to the utility of PCL in other medical devices and drug delivery systems.[85, 86] PCL's low T_g (-60 °C) permits the formation of elastic rather than rigid networks. PCL is an effective switching segment in which the T_m forms the T_{trans} of the network. Linear PCLs exhibit well-defined T_m's which decrease with their M_n (43 – 60 °C).[68] Furthermore, the low T_m's of PCL are desirable in biomedical applications. These unique qualities has prompted the investigation of SMPs formed by combination of PCL with a variety of organic

copolymers, including: polyurethanes,[84, 87-89] poly(*n*-butyl acrylate),[90] poly(L-lactide),[49, 91-93] poly(glycolide),[94] and poly(ethylene glycol).[95]

SMPs, including those based on PCL, have been traditionally fabricated from purely organic polymer systems. However, polymers and networks prepared from a combination of inorganic and organic polymers often leads to unique material properties. Polydimethylsiloxane (PDMS) has many interesting properties, including good biocompatibility, thermal and oxidative stability, gas permeability and an extremely low T_g (-125 °C).[96, 97] The low T_g of PDMS leads to highly elastic networks upon lightly crosslinking. Thus, modification of organic biodegradable polymers with PDMS to confer elasticity has received interest for TE scaffolds and soft microcapules used in oral drug delivery.[98] A single report of SMPs formed by radiation crosslinking of physical blends of PCL and polymethylvinylsiloxane (PMVS) has appeared.[99] However, blends could only be prepared with less than 20 wt% of PMVS due to blend instability. Furthermore, PCL is susceptible to radiation-induced chain scission which diminishes tensile strength.

In this study, we have designed novel inorganic-organic biodegradable elastomers useful as TE scaffolds or SMPs. These elastomers were formed through rapid photochemical cure of a series of photosensitive block copolymer macromers consisting of a central inorganic PDMS block and terminal organic PCL blocks: AcO-PCL_n-*block*-$PDMS_m$-*block*-PCL_n-OAc. Thermoplastic block copolymers of PDMS and PCL have been previously reported but were not subsequently functionalized with crosslinkable endgroups and converted into networks.[100-104] A macromer with a block

structure will maintain the properties of PCL and PDMS components desirable for biodegradable elastomers. PCL blocks will introduce biodegradability, elasticity, and may serve as switching segments if shape memory behavior is desired. PDMS segment should confer greater elasticity to the PCL-based network.[98] In addition, block copolymers may also produce periodic nanostructures resulting in amphiphilic characteristics and unique surface properties.[52] Our synthetic strategy also permits the systematic control of M_n of the PDMS and PCL blocks and hence PDMS:PCL ratios and crosslink density. As a photo-crosslinked system, elastomers cure is rapid and permits spatial and temporal control.[105] In addition, porosity may be introduced into these elastomers by photocuring in the presence of porogens (as discussed in Chapter III). Porosity ensures substantial surface area for cell growth and attachment for TE scaffolds and could also be used to prepare SMP foams. In this study, we maintained the M_n of the PDMS block (m = 37) while systematically altering that of the PCL blocks (n = 5, 10, 20, 30 and 40) which led to changes in the PDMS:PCL ratios and crosslink density. The effect of these structural changes on thermal, surface, mechanical, and shape memory properties were studied.

2.2 Experimental Section

Polymer Characterization

NMR Spectroscopy. ^{1}H NMR spectra were obtained on an Inova 300-MHz spectrometer operating in the FT mode. Five percent w/v $CDCl_3$ solutions were used. Residual $CDCl_3$ served as an internal standard.

Thermal Gravimetric Analysis (TGA). The thermal stabilities of neat samples (~15 mg) in Pt pans were evaluated with a TA Instruments Q50 under N_2 or air at a flow rate of 40 cc/min. The sample weight was recorded while the temperature was increased 10 ˚C/min from 25 to 800 ˚C.

Elastomer Characterization

Thermal Gravimetric Analysis (TGA). Thermal analysis of photocured elastomers (~15 mg) were similarly measured as described above.

Sol Content. Uncrosslinked material (sol) was extracted by soaking an elastomer disc (45 mm x 2mm; ~0.70 g) in a sealed vial containing 15 mL of ethanol and placing on a shaker table for 3 hrs. The percentage of uncrosslinked material was calculated as $(w_0-w_1)/w_0$, where w_0 is weight before extraction and w_1 is weight after extraction.

Dynamic Mechanical Analysis (DMA). Storage (G') and loss (G") moduli of elastomers were measured as a function of temperature on a TA Instruments Q800 dynamic mechanical analyzer. Specimens (length x width = 35 mm x 5.3 mm) were cut from an elastomer disc using a clean single-edged razor cutting tool. Electronic calipers were used to measure film thickness (~ 1.0 mm) prior to testing. The DMA was operated using a dual cantilever clamp assembly at a frequency of 5 Hz and a displacement of 4 μm. After equilibration at -140 °C for 3 min, the temperature was increased 4 ˚C/min to 95 ˚C. The T_g was determined from the peak maximum of the measured G".

Contact Angle Analysis. The surfaces of elastomers were characterized using a KSV CAM-200 contact angle measurement system equipped with an autodispenser,

video camera, and drop-shape analysis software. Static (θ_{static}), advancing (θ_{adv}), and receding (θ_{rec}) contact angle measurements of distilled/deionized water droplets at the elastomer-air interface were measured at room temperature. For θ_{static}, a 5 μL sessile drop of water was measured at 15 sec and 2 min after deposition onto the elastomer surface. The θ_{adv} was measured by the addition of 3 μL (0.25 μL/s) of water to a 5 μL pendant droplet to advance the contact line. The θ_{rec} was measured by the subsequent removal of 4 μL (0.25 μL/s) from the same droplet to recede the contact line. The reported θ_{static}, θ_{adv}, and θ_{rec} values are an average of three measurements taken on different areas of the same elastomer sample.

Tensile Properties. Rectangular strips (20 mm x 3.3 mm x 1.1 mm) were subjected to tensile tests using an Instron 3340 universal testing machine. Samples were subjected to a constant strain (50 mm/min) until they broke. Young's modulus (E), tensile strength (T.S.), and percent strain at break (%ε) were determined from resulting stress (σ) vs. strain (ε) curves. Measurements were performed in triplicate.

Differential Scanning Calorimetry (DSC). The melting temperature (T_m) and heat of fusion (ΔH_m) were determined by differential scanning calorimetry (DSC, TA Instruments Q100). The cell was calibrated using an indium standard and sample weight was ~ 12 mg. After equilibration at -150 °C for 5 min, the temperature was increased to 95 °C at a rate of 5 °C/min for one cycle. The endothermic melting peak was characterized by a peak minimum (T_m) and enthalpy change (ΔH_m). The crystalline fraction, χ_c, was calculated as follows:

$$\chi_c = \frac{\Delta H_m}{\Delta H_m^0} \quad (1)$$

where ΔH_m was calculated by area of the melting peak and ΔH^0_m is the enthalpy of fusion of 100% crystalline PCL. A value of ΔH^0_m = 139.5 J/g was used for the calculation.[106, 107] In this way, percent crystallinity (χ_c x 100) was determined.

Thermomechanical Characterization. Cyclic thermomechanical tests were carried out on a dynamic mechanical analyzer (TA Instruments Q800). Rectangular strips (15 mm x 3 mm x 1.1 mm) mounted onto tension clamps (gauge length = 6.5 mm) were subjected to the following sequence: (1) after equilibrating at 80 °C (T_{high}) for 10 min, elongate to a maximum strain (ε_m = 75%) at a rate of 50% strain/min (or 3.1 mm/min), (2) hold at ε_m for 5 min and then cool to 25 °C (T_{low}) to fix the temporary shape, (3) remove load and immediately measure ε_u, (4) reheat the sample to 80 °C (T_{high}) to recover to the permanent shape and measure ε_p, then begin the second cycle. In total, 4 cycles were performed.

The shape memory effect was quantified by two values: strain recovery (R_r) and strain fixity (R_f). For each cycle (N), strain recovery rate (R_r) quantifies the ability of a material to return to its permanent shape (ε_p) after application of mechanical deformation (ε_m). Specifically, it is a measure of how much of the strain applied in the course of programming ε_m - $\varepsilon_p(N-1)$ is recovered in the following shape-memory transition ε_m - $\varepsilon_p(N)$. Thus, R_r is defined as:

$$R_r(N) = \frac{\varepsilon_m - \varepsilon_p(N)}{\varepsilon_m - \varepsilon_p(N-1)} \quad (2)$$

where ε_m is the maximum strain induced and $\varepsilon_p(N-1)$ and $\varepsilon_p(N)$ are the strain of the sample in two successively passed cycles in the stress-free state. Total strain recovery rate ($R_{r,tot}$) is defined as the total recovered strain for each independent cycle ($\varepsilon_p(N)$) as compared to the original strain deformation (ε_m):

$$R_{r,tot} = \frac{\varepsilon_m - \varepsilon_p(N)}{\varepsilon_m} \tag{3}$$

Strain fixity (R_f) quantifies the ability of the material to maintain or fix a mechanical deformation (ε_m) after cooling resulting in a temporary deformation (ε_u):

$$R_f = \frac{\varepsilon_u(N)}{\varepsilon_m} \tag{4}$$

where, ε_u is the sample's strain immediately following unloading. Ideally, R_r and R_f should be 100%.

Macroscopic Shape Memory Effect. The shape memory effect was captured photographically. The rectangular strip (25 mm x 3 mm x 1.1 mm) was deformed to a temporary coil by heating to 80 °C, stretching to 150%, wrapping around a steel rod (~2 mm dia.), and cooled in an ice bath to lock in temporary shape. The resulting coil was blotted dry and placed in an oven or in DI water maintained at 40, 50, or 60 °C.

Time series photographs captured time-lapse from deformed, temporary shape (coil) to the undeformed, permanent shape (flat rectangle).

2.3 Materials

ε-Caprolactone, triethylamine (Et_3N), acryloyl chloride, stannous 2-ethylhexanoate, 2,2-dimethoxy-2-phenyl-acetophenone (DMAP), 1-vinyl-2-pyrrol-idinone (NVP), 4-(dimethylamino)-pyridine (DMP), K_2CO_3, Poly(dimethylsiloxane)-bis(3-aminopropyl) terminated (NH_2-$PDMS_{37}$-NH_2; M_n ~ 3,000 g/mol per manufacturers specifications; 2986 g/mol as determined by ^1H NMR end group analysis), and solvents were obtained from Sigma Aldrich. Anhydrous magnesium sulfate ($MgSO_4$) was obtained from Fisher. Reagent-grade CH_2Cl_2, $CHCl_3$, and NMR grade $CDCl_3$ were dried over 4Å molecular sieves.

2.4 Synthetic Approach

The HO-PCL_n-*block*-$PDMS_{37}$-*block*-PCL_n-OH macromers were prepared by ring-opening polymerization of ε-caprolactone in the presence of a tin catalyst and NH_2-$PDMS_{37}$-NH_2 (Fig. 2.1). The M_n of the PCL blocks was controlled by the ratio of ε-caprolactone to NH_2-$PDMS_{37}$-NH_2. The NH_2-$PDMS_{37}$-NH_2, ε-caprolactone, and stannous 2-ethylhexanoate catalyst were combined into a 250 mL round-bottomed (rb) flask equipped with rubber septum and magnetic Teflon stir bar. The reaction was stirred for 24 h at 145 °C under N_2. After cooling to room temperature (RT), the crude product was dissolved in minimal amount of $CHCl_3$ and precipitated twice in an excess of cold

methanol (~10 °C). The isolated product was dried under high vacuum at 45°C for 20 h. PDMS:PCL ratio and M_n were determined by ^{1}H NMR spectroscopy.

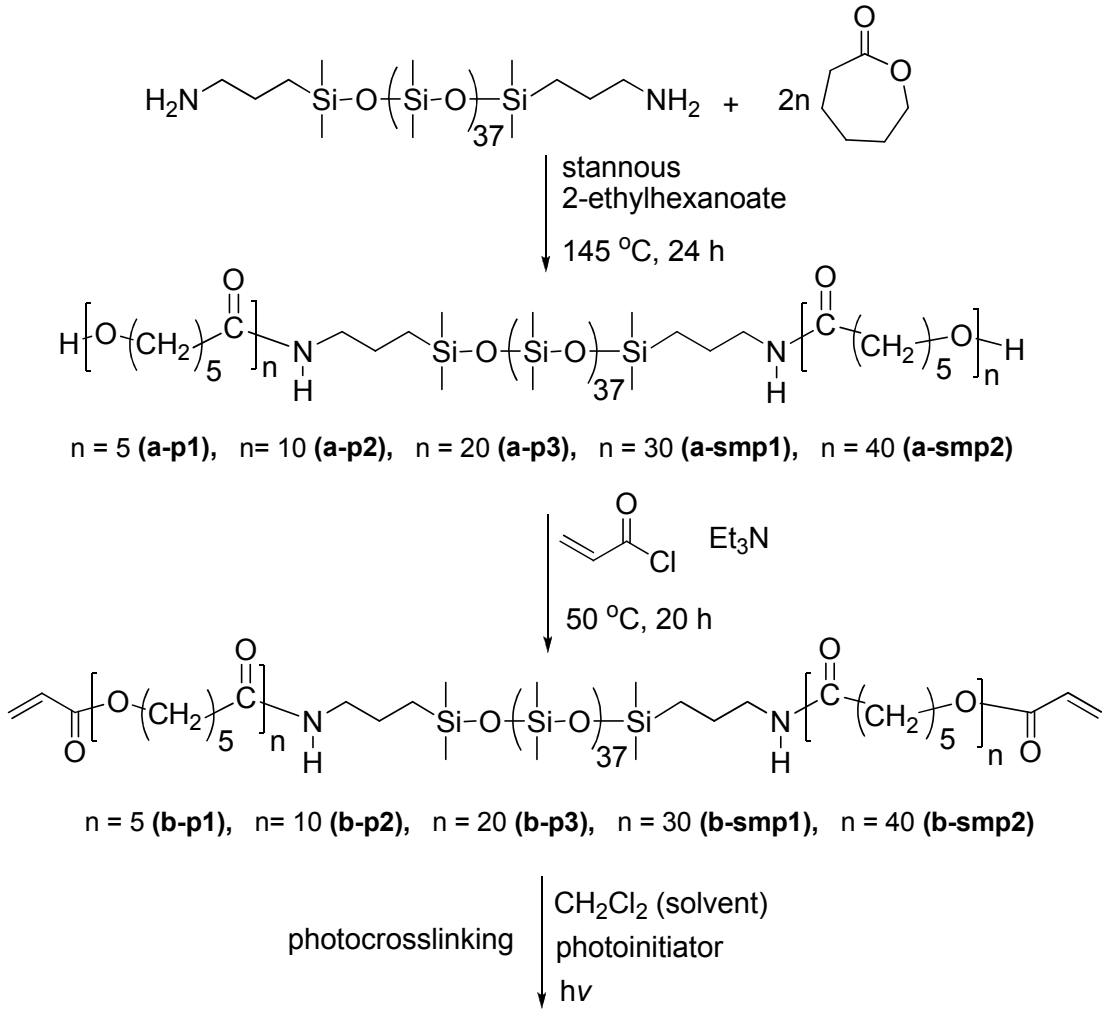

Figure 2.1. Synthesis of photocurable AcO-PCL$_n$-*block*-PDMS$_{37}$-*block*-PCL$_n$-OAc macromers and their conversion to **P1-3** and **SMP1-2** elastomers. **SMP1** and **SMP2** exhibit shape memory behavior.

The terminal hydroxyl groups were subsequently converted to photosensitive acrylate (OAc) groups by reaction with acryloyl chloride to yield AcO-PCL_n-*block*-$PDMS_m$-*block*-PCL_n-OAc macromers (Fig. 2.1). Each were combined with DMP, and dry CH_2Cl_2 and placed in a 250 mL rb flask equipped with a Teflon stir bar, rubber septum, and purged with N_2. Et_3N was slowly added to the solution followed by the dropwise addition of acryloyl chloride. After 30 min, the mixture was refluxed at 50 °C for 20 h with mild stirring. The solvent was removed under reduced pressure, the crude product dissolved in ethyl acetate and filtered to remove triethylamine hydrochloride salts. After removing solvent under reduced pressure, the isolated product was dissolved in CH_2Cl_2 (125 – 140 mL), and washed with 2 M K_2CO_3 (12 mL). The isolated organic layer was dried with $MgSO_4$, gravity filtered, and volatiles removed under reduced pressure. ^{1}H NMR spectroscopy confirmed acrylation as well as maintenance of PDMS:PCL ratio and M_n.

Synthesis of Hydroxy Terminated Biodegradable Macromers

Synthesis of HO-PCL_5-*block*-$PDMS_{37}$-*block*-PCL_5-OH (**a-p1**). NH_2-$PDMS_{37}$-NH_2 (20.0 g, 6.69 mmol), ε-caprolactone (7.17 g, 66.67 mmol), and stannous 2-ethylhexanoate catalyst (0.043 g, 0.11 mmol) were reacted as above. In this way, **a-p1** (19.33 g, 70% yield) was obtained as a viscous, yellowish liquid. M_n= 3,965 g/mol (by ^{1}H NMR end group analysis). ^{1}H NMR (δ, ppm): 0.11 – 0.40 (bm, 240H, Si*CH*$_3$), 0.49 (m, 3H, -SiC*H*$_2$$CH_2CH_2NH$-), 1.35 (m, 18H, -$OCH_2CH_2CH_2CH_2CH_2OH$), 1.58 (m, 40H, -$COCH_2CH_2CH_2CH_2CH_2OH$), 2.11 (m, 4H, -$SiCH_2CH_2CH_2NH$-), 2.27

(m, 14H, -COC*H*$_2$CH$_2$CH$_2$CH$_2$CH$_2$OH), 3.19 (q, *J* = 6 Hz, 4H, -SiCH$_2$CH$_2$C*H*$_2$NH-), 3.61 (t, *J* = 6 Hz, 2H, N*H*), 4.02 (m, 14H, -COCH$_2$CH$_2$CH$_2$CH$_2$C*H*$_2$OH).

Synthesis of HO-PCL$_{10}$-*block*-PDMS$_{37}$-*block*-PCL$_{10}$-OH (**a-p2**). NH$_2$-PDMS$_{37}$-NH$_2$ (15.0 g, 5.0 mmol), ε-caprolactone (10.76 g, 100 mmol), and stannous 2-ethylhexanoate catalyst (0.043 g, 0.11 mmol) were reacted as above. In this way, **a-p2** (24.88 g, 94% yield) was obtained as a viscous, yellowish liquid. M_n= 5,170 g/mol (by ^{1}H NMR end group analysis). ^{1}H NMR (δ, ppm): 0.35 – 0.11 (bm, 240H, Si*CH*$_3$), 0.49 (m, 4H, -SiC*H*$_2$CH$_2$CH$_2$NH-), 1.39 (m, 41H, -OCH$_2$CH$_2$CH$_2$C*H*$_2$CH$_2$OH), 1.58 (m, 82H, -COCH$_2$C*H*$_2$C*H*$_2$CH$_2$CH$_2$OH), 2.11 (m, 4H, -SiCH$_2$C*H*$_2$CH$_2$NH-), 2.27 (m, 36H, -COC*H*$_2$CH$_2$CH$_2$CH$_2$CH$_2$OH), 3.19 (q, *J* = 6.6 Hz, 4H, -SiCH$_2$CH$_2$C*H*$_2$NH-), 3.61 (t, *J* = 6.6, 2H, N*H*), 4.02 (m, 33H, -COCH$_2$CH$_2$CH$_2$CH$_2$C*H*$_2$OH).

Synthesis of HO-PCL$_{20}$-*block*-PDMS$_{37}$-*block*-PCL$_{20}$-OH (**a-p3**). NH$_2$-PDMS$_{37}$-NH$_2$ (7.57 g, 2.54 mmol), ε-caprolactone (10.85 g, 100.8 mmol), and stannous 2-ethylhexanoate catalyst (0.043 g, 0.11 mmol) were reacted as above. In this way, **a-p3** (14.37 g, 74% yield) was obtained as a yellowish wax. M_n= 7,750 g/mol (by ^{1}H NMR end group analysis). ^{1}H NMR (δ, ppm): 0.03 – 0.11 (bm, 240H, Si*CH*$_3$), 0.49 (m, 4H, -SiC*H*$_2$CH$_2$CH$_2$NH-), 1.39 (m, 89H, -COCH$_2$CH$_2$CH$_2$C*H*$_2$CH$_2$OH), 1.58 (m, 174H, -COCH$_2$C*H*$_2$C*H*$_2$CH$_2$CH$_2$OH), 2.11 (m, 4H, -SiCH$_2$C*H*$_2$CH$_2$NH-), 2.27 (m, 78H, -COC*H*$_2$CH$_2$CH$_2$CH$_2$CH$_2$OH), 3.19 (q, *J* = 6.6 Hz, 4H, -SiCH$_2$CH$_2$C*H*$_2$NH-), 3.61 (t, *J* = 6.6 Hz, 2H, N*H*), 4.02 (m, 77H, -COCH$_2$CH$_2$CH$_2$CH$_2$C*H*$_2$OH).

Synthesis of HO-PCL$_{30}$-*block*-PDMS$_{37}$-*block*-PCL$_{30}$-OH (**a-smp1**). NH$_2$-PDMS$_{37}$-NH$_2$ (5.0 g, 1.67 mmol), ε-caprolactone (10.78 g, 100.21 mmol), and

stannous 2-ethylhexanoate catalyst (0.043 g, 0.11 mmol) were reacted as above. In this way, **a-smp1** (10.36 g, 63% yield) was obtained as a yellowish wax. M_n= 9,980 g/mol (by ^{1}H NMR end group analysis). ^{1}H NMR (δ, ppm): 0.03 – 0.12 (bm, 240H, Si*CH*$_3$), 0.49 (m, 4H, -SiC*H*$_2$CH$_2$CH$_2$NH-), 1.39 (m, 120H, -COCH$_2$CH$_2$CH$_2$C*H*$_2$CH$_2$OH), 1.58 (m, 252H, -COCH$_2$C*H*$_2$C*H*$_2$CH$_2$CH$_2$OH), 2.11 (m, 4H, -SiCH$_2$C*H*$_2$CH$_2$NH-), 2.27 (m, 123H, -COC*H*$_2$CH$_2$CH$_2$CH$_2$CH$_2$OH), 3.19 (q, *J* = 6.6 Hz, 4H, -SiCH$_2$CH$_2$C*H*$_2$NH-), 3.61 (t, *J* = 6.6 Hz, 2H, N*H*), 4.02 (m, 118H, -COCH$_2$CH$_2$CH$_2$CH$_2$C*H*$_2$OH).

Synthesis of HO-PCL$_{40}$-*block*-PDMS$_{37}$-*block*-PCL$_{40}$-OH (**a-smp2**). NH$_2$-PDMS$_{37}$-NH$_2$ (6.71 g, 2.25 mmol), ε-caprolactone (19.26 g, 179.0 mmol), and stannous 2-ethylhexanoate catalyst (0.043 g, 0.11 mmol) were reacted as above. In this way, **a-smp2** (20.25 g, 75% yield) was obtained as a yellowish wax. M_n= 11,940 g/mol (by ^{1}H NMR end group analysis). ^{1}H NMR (δ, ppm): 0.03 – 0.13 (bm, 240H, Si*CH*$_3$), 0.49 (m, 4H, -SiC*H*$_2$CH$_2$CH$_2$NH-), 1.39 (m, 161H, -COCH$_2$CH$_2$CH$_2$C*H*$_2$CH$_2$OH), 1.58 (m, 323H, -COCH$_2$C*H*$_2$C*H*$_2$CH$_2$CH$_2$OH), 2.11 (m, 4H, -SiCH$_2$C*H*$_2$CH$_2$NH-), 2.27 (m, 153H, -COC*H*$_2$CH$_2$CH$_2$CH$_2$CH$_2$OH), 3.19 (q, *J* = 6.6 Hz, 4H, -SiCH$_2$CH$_2$C*H*$_2$NH-), 3.61 (t, *J* = 6.6 Hz, 2H, N*H*), 4.02 (m, 149H, -COCH$_2$CH$_2$CH$_2$CH$_2$C*H*$_2$OH).

Synthesis of Photosensitive Acrylated Biodegradable Macromers

Synthesis of AcO-PCL$_5$-*block*-PDMS$_{37}$-*block*-PCL$_5$-OAc (**b-p1**). **a-p1** (19.33 g, 4.49 mmol), DMP (0.0023 g, 0.02 mmol), Et$_3$N (0.909 g, 8.99 mmol), acryloyl chloride (1.62 g, 17.98 mmol) were reacted as above. In this way, **b-p1** (15.29 g, 80% yield) was obtained as a tacky, yellowish solid. M_n = 4,055 g/mol (by ^{1}H NMR end group

analysis). ^{1}H NMR (δ, ppm): 0.03 – 0.11 (bm, 240H, Si*CH*$_3$), 0.49 (m, 4H, -SiC*H*$_2$CH$_2$CH$_2$NH-), 1.39 (m, 20H, -COCH$_2$CH$_2$CH$_2$C*H*$_2$CH$_2$OH), 1.58 (m, 40H, -COCH$_2$C*H*$_2$C*H*$_2$CH$_2$CH$_2$OH), 2.11 (m, 4H, -SiCH$_2$C*H*$_2$CH$_2$NH-), 2.27 (m, 14H, -COC*H*$_2$CH$_2$CH$_2$CH$_2$CH$_2$OH), 3.19 (q, *J* = 6.9 Hz, 4H, -SiCH$_2$CH$_2$C*H*$_2$NH-), 3.61 (m, 2H, N*H*), 4.02 (m, 12H, -COCH$_2$CH$_2$CH$_2$CH$_2$C*H*$_2$OH), 5.82 (dd, 2H, *J* = 1.5 and 10.5 Hz, -COCCHC*H*$_2$), 6.11 (dd, 2H, *J* = 10.5 and 17.4 Hz, -COCC*H*CH$_2$), 6.40 (dd, 2H, *J* = 1.8 and 17.4 Hz, -COCCHC*H*$_2$).

Synthesis of AcO-PCL$_{10}$-*block*-PDMS$_{37}$-*block*-PCL$_{10}$-AcO **(b-p2).** **a-p2** (24.88 g, 4.87 mmol), DMP (.0023 g, 0.02 mmol), Et$_3$N (0.985 g, 9.74 mmol), acryloyl chloride (1.76 g, 19.48 mmol) were reacted as above. In this way, **b-p2** (17.40 g, 66% yield) was obtained as a tacky, yellowish solid. M_n = 5,250 g/mol (by ^{1}H NMR end group analysis). ^{1}H NMR (δ, ppm): 0.05 – 0.11 (bm, 240H, Si*CH*$_3$), 0.49 (m, 4H, -SiC*H*$_2$CH$_2$CH$_2$NH-), 1.39 (m, 40H, -COCH$_2$CH$_2$CH$_2$C*H*$_2$CH$_2$OH), 1.58 (m, 83H, -COCH$_2$C*H*$_2$C*H*$_2$CH$_2$CH$_2$OH), 2.11 (m, 4H, -SiCH$_2$C*H*$_2$CH$_2$NH-), 2.27 (m, 35H, -COC*H*$_2$CH$_2$CH$_2$CH$_2$CH$_2$OH), 3.19 (q, *J* = 6.9 Hz, 4H, -SiCH$_2$CH$_2$C*H*$_2$NH-), 3.61 (m, 2H, N*H*), 4.02 (m, 31H, -COCH$_2$CH$_2$CH$_2$CH$_2$C*H*$_2$OH), 5.82 (dd, 2H, *J* = 1.8 and 10.5 Hz, -COCCHC*H*$_2$), 6.11 (dd, 2H, *J* = 10.5 and 17.4 Hz, -COCC*H*CH$_2$), 6.40 (dd, 2H, *J* = 1.7 and 17.3 Hz, -COCCHC*H*$_2$).

Synthesis of AcO-PCL$_{20}$-*block*-PDMS$_{37}$-*block*-PCL$_{20}$-OAc (**b-p3**). **a-p3** (14.37 g, 1.84 mmol), DMP (0.0023 g, 0.02 mmol), Et$_3$N (0.372 g, 3.68 mmol), acryloyl chloride (0.664 g, 7.37 mmol) were reacted as above. In this way, **b-p3** (5.02 g, 37% yield) was obtained as a tacky, yellowish solid. M_n = 7,880 g/mol (by ^{1}H NMR end

group analysis). ^{1}H NMR (δ, ppm): 0.05 – 0.11 (bm, 240H, Si*CH*$_3$), 0.49 (m, 4H, -SiC*H*$_2$CH$_2$CH$_2$NH-), 1.39 (m, 86H, -COCH$_2$CH$_2$CH$_2$C*H*$_2$CH$_2$OH), 1.58 (m, 185H, -COCH$_2$C*H*$_2$C*H*$_2$CH$_2$CH$_2$OH), 2.11 (m, 4H, -SiCH$_2$C*H*$_2$CH$_2$NH-), 2.27 (m, 78H, -COC*H*$_2$CH$_2$CH$_2$CH$_2$CH$_2$OH), 3.19 (m, 4H, -SiCH$_2$CH$_2$C*H*$_2$NH-), 3.61 (m, 2H, N*H*), 4.02 (m, 74H, -COCH$_2$CH$_2$CH$_2$CH$_2$C*H*$_2$OH), 5.82 (dd, 2H, *J* = 1.5 and 10.5 Hz, -COCCHC*H*$_2$), 6.11 (dd, 2H, *J* = 10.5 and 17.4 Hz, -COCC*H*CH$_2$), 6.40 (dd, 2H, *J* = 1.5 and 17.4 Hz, -COCCHC*H*$_2$).

Synthesis of AcO-PCL$_{30}$-*block*-PDMS$_{37}$-*block*-PCL$_{30}$-OAc (**b-smp1**). **a-smp1** (10.36 g, 1.04 mmol), DMP (0.0023 g, 0.02 mmol), Et$_3$N (0.210 g, 2.07 mmol), acryloyl chloride (0.374 g, 4.14 mmol) were reacted as above. In this way, **b-smp1** (4.73 g, 46% yield) was obtained as a waxy, yellowish solid. M_n = 9,860 g/mol (by ^{1}H NMR end group analysis). ^{1}H NMR (δ, ppm): 0.008 – 0.14 (bm, 240H, Si*CH*$_3$), 0.49 (m, 1H, -SiC*H*$_2$CH$_2$CH$_2$NH-), 1.39 (m, 130H, -COCH$_2$CH$_2$CH$_2$C*H*$_2$CH$_2$OH), 1.58 (m, 244H, -COCH$_2$C*H*$_2$C*H*$_2$CH$_2$CH$_2$OH), 2.11 (m, 4H, -SiCH$_2$C*H*$_2$CH$_2$NH-), 2.27 (m, 114H, -COC*H*$_2$CH$_2$CH$_2$CH$_2$CH$_2$OH), 3.19 (m, 4H, -SiCH$_2$CH$_2$C*H*$_2$NH-), 3.61 (m, 2H, N*H*), 4.02 (m, 106H, -COCH$_2$CH$_2$CH$_2$CH$_2$C*H*$_2$OH), 5.82 (dd, 2H, *J* = 1.5 and 10.2 Hz, -COCCHC*H*$_2$), 6.11 (dd, 2H, *J* = 10.5 and 17.4 Hz, -COCC*H*CH$_2$), 6.40 (dd, 2H, *J* = 1.8 and 17.7 Hz, -COCCHC*H*$_2$).

Synthesis of AcO-PCL$_{40}$-*block*-PDMS$_{37}$-*block*-PCL$_{40}$-OAc (**b-smp2**). **a-smp2** (20.25 g, 1.70 mmol), DMP (0.0023 g, 0.02 mmol), Et$_3$N (0.343 g, 3.39 mmol), acryloyl chloride (0.612 g, 6.78 mmol) were reacted as above. In this way, **b-smp2** (11.44 g, 55% yield) was obtained as a waxy, yellowish solid. M_n = 11,990 g/mol (by ^{1}H NMR).

^{1}H NMR (δ, ppm): 0.046 - 0.10 (bm, 240H, SiCH_3), 0.49 (m, 4H, -SiCH_2CH$_2$CH$_2$NH-), 1.39 (m, 165H, -COCH$_2$CH$_2$CH$_2$CH_2CH$_2$OH), 1.58 (m, 327H, -COCH$_2$CH_2CH_2CH$_2$CH$_2$OH), 2.11 (m, 4H, -SiCH$_2$CH_2CH$_2$NH-), 2.27 (m, 148H, -COCH_2CH$_2$CH$_2$CH$_2$CH$_2$OH), 3.19 (m, 4H, -SiCH$_2$CH$_2$CH_2NH-), 3.61 (m, 2H, NH), 4.02 (m, 143H, -COCH$_2$CH$_2$CH$_2$CH$_2$CH_2OH), 5.82 (dd, 2H, J = 1.5 and 10.4 Hz, -COCCHCH_2), 6.11 (dd, 2H, J = 10.5 and 17.4 Hz, -COCCHCH$_2$), 6.40 (dd, 2H, J = 1.8 and 17.4 Hz, -COCCHCH_2).

2.5 Preparation of Biodegradable Elastomers

The photosensitive macromers (**b-P1-P3; b-SMP1-SMP2**) were photochemically crosslinked into elastomers (**P1-P3; SMP1-SMP2**) using a photoinitiator consisting of 10 wt% solution of DMAP in NVP. A precursor solution was prepared by dissolving acrylated macromers in CH_2Cl_2 at 0.25 g/mL, 0.5 g/mL, or 1 g/mL in a scintillation vial. Photoinitiator solution was then added at a volume of 150 μL per mL of CH_2Cl_2. After vortexing, the solution was transferred to the well of a circular silicone isolator (45 mm x 2 mm) sandwiched between two glass slides (Fig. 2.2). The mold was then exposed to UV light (UV-Transilluminator, 6 mW/cm^2, 365 nm) for 3 min to form an elastomer network. The resulting solvent-swollen elastomer disc was removed from the mold, air dried (RT, 12 h), and dried *in vacuo* (36" Hg, 80 °C, 4 h) to remove residual solvent. Uncrosslinked material (sol) was removed by soaking the disc in ethanol (~3 h), air drying overnight, and drying *in vacuo* as above. In

this way, a series of elastomers **(P1-P3, SMP1-SMP2)** were prepared at different concentrations (Table 2.1).

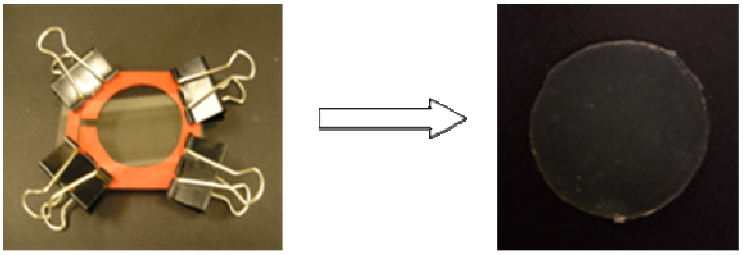

Figure 2.2. Elastomer discs were formed by filling sandwich molds with precursor solution and exposing to UV light for 3 min.

Table 2.1. Elastomer notation and corresponding macromer structure

Elastomer	Structure	% PCL	M_n g/mol (theoretical)	M_n g/mol (^{1}H NMR)
P1	PCL_5-*block*-$PDMS_{37}$-*block*-PCL_5	21%	4,234	4,055
P2	PCL_{10}-*block*-$PDMS_{37}$-*block*-PCL_{10}	35%	5,374	5,250
P3	PCL_{20}-*block*-$PDMS_{37}$-*block*-PCL_{20}	60%	7,654	7,880
SMP1*	PCL_{30}-*block*-$PDMS_{37}$-*block*-PCL_{30}	69%	9,934	9,860
SMP2*	PCL_{40}-*block*-$PDMS_{37}$-*block*-PCL_{40}	75%	12,214	11,990

* Exhibits shape memory effect
All elastomers prepared at c = 0.25 g/mL
P1, P2, SMP1 also prepared at c = 0.5 g/mL, 1 g/mL

2.6 Results and Discussion

A series of triblock biodegradable elastomers composed of PCL and PDMS blocks were developed. First, by controlling the molar ratio of NH_2-$PDMS_{37}$-NH_2 to ε-caprolactone during synthesis, a series of HO-PCL_n-*block*-$PDMS_{37}$-*block*-PCL_n-OH macromers were created with different % PCL content and M_n. Terminal hydroxyl

groups were subsequently converted to photosensitive acrylate group by reaction with acryloyl chloride to yield AcO-PCL_n-*block*-$PDMS_{37}$-*block*-PCL_n-OAc macromers. Acrylated macromers were dissolved in CH_2Cl_2 and crosslinked in the presence of a photoinitiator. Resulting elastomers varied in PCL content and crosslink density was changed by M_n of acrylated monomers as well as concentration of precursor solutions upon crosslinking. Thermal, tensile, surface, and shape memory properties were investigated for all synthesized elastomers.

Thermal Properties

As potential SMP's, these elastomers must exhibit a T_{trans}, above which the network switches from temporary to permanent shape. For these elastomers, the PCL blocks may serve as the switching segment and its melting temperature (T_m) would be T_{trans}. For PCL, the T_m = 43 – 60 °C and decreases as M_n increases.[68] Parameters for PCL-based SMP have been previously reported: 40 to 55 °C (T_m), 33 – 52 J/g (ΔH_m), and 20 – 38% (χ_c) and are dependent on chemical structure, molecular weight, and associated copolymer.[49, 90, 108]

DSC was used to measure T_m, ΔH_m, and % crystallinity (χ_c) of these elastomers (Table 2.2; Fig. 2.3A). Elastomer networks **P1-P2** exhibited no melting transition whereas **P3** and **SMP1-SMP2** did. The PCL block lengths of **P1** (n = 5) and **P2** (n = 10) were apparently too short to develop crystalline domains. **P3** (n = 20) exhibited a T_m at 33 °C. However, the value of ΔH_m (1.7 J/g) and % crystallinity (1.2%) of **P3** were quite small. On the other hand, **SMP1** (n = 30) and **SMP2** (n = 40) exhibited a T_m at 52 and 50

°C, respectively. Furthermore, they exhibited substantially higher % crystallinity of 29% (ΔH_m = 41 J/g) and 26% (ΔH_m = 36 J/g), respectively. The increased level of crystallinity is clearly visible as elastomers transition from clear to opaque with increasing PCL M_n (Fig. 2.3B).

Table 2.2. Elastomer thermal properties

Elastomer	T_g (°C)	T_m (°C)	ΔH_m (J/g)	Crystallinity (%)	Visual Appearance
P1	-114, -46	- -	- -	0	clear
P2	-113, -50	- -	- -	0	clear
P3	-115, -50	33	1.7	1.2	hazy
SMP1	-120, -35	52	41	29	opaque
SMP2	-120, -48	50	36	26	opaque

Prepared at conc. = 0.25 g/mol.

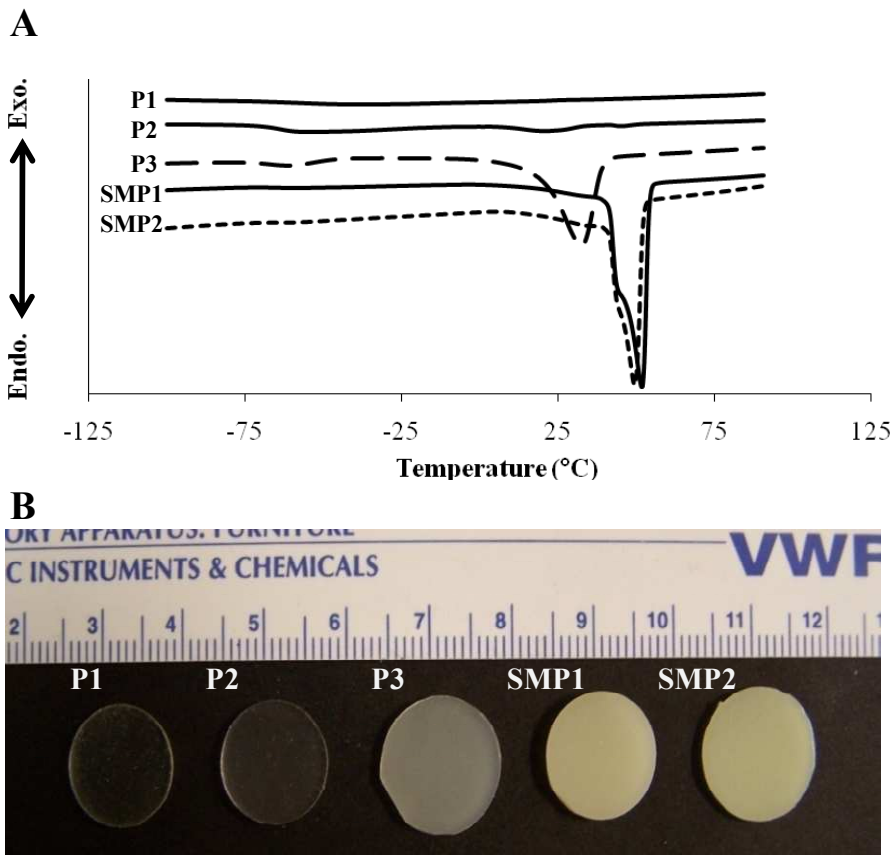

Figure 2.3. **A**) DSC curve demonstrating melting temperature T_m. **B**) Elastomer discs became more opaque as PCL segment crystallinity increased with M_n.

The T_g of the biodegradable elastomers were investigated using DMA (Table 2.2). Two distinct T_g's were observed for all DMA tests using maxima of G" peaks (Fig. 2.4).[109] Observation of two T_g's is typical for block copolymer structures.[110-112] In these elastomers, the PCL and PDMS blocks are of sufficient length to exhibit separate T_g's. The T_g observed at -113 to -120 °C is attributed to the PDMS block and is slightly higher than the T_g of thermoplastic PDMS (-125 °C).[113, 114] The second T_g observed at -35 to -50 °C is due to the PCL block and is slightly higher than the T_g of thermoplastic PCL (-55 to -65 °C).[115-117] Since these T_g's are well below both body and room temperature, these materials are expected to behave elastically at these temperatures.

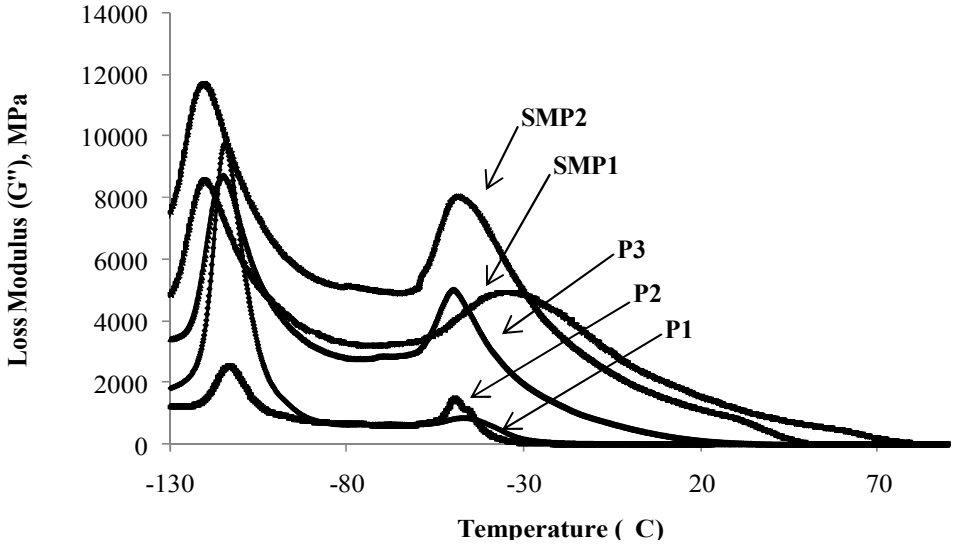

Figure 2.4. Loss modulus (G'') versus Temperature (°C). Maxima of peaks represent T_g's of elastomers.

Tensile Properties

The mechanical properties of elastomers were characterized by tensile tests at room temperature. First, to evaluate the influence of PCL content and crosslink density, elastomers were prepared at a single concentration (0.25 g/mL) (Table 2.3). The tensile modulus and tensile strength of **P3**, **SMP1**, and **SMP2** increased by a factor of 10 versus that of **P1** and **P2**. In addition, large increases in % strain at break were noted as the M_n of PCL blocks increased and reached 814% for **SMP2**. Typically, polymers with lower crosslink density will display increased strain at break with concomitant decrease in tensile modulus and tensile strength. However, for these elastomers all mechanical properties increase despite the decrease in crosslink density. This phenomena is attributed to the development of crystalline domains. **SMP1** (29%) and **SMP2** (26%) exhibited significantly higher percent crystallinity versus **P3** (1.7%) and **P1** and **P2** were amorphous. Thus, as PCL M_n and content increase, enhanced crystallinity led to increased tensile modulus and tensile strength. Enhanced crystallinity is well-known to increase strength and rigidity of semi-crystalline polymers because crystalline lamellae act as physical crosslinks.

Table 2.3 Tensile properties at room temperature

Elastomer	Block Length (n) M_n (g/mol)	Tensile Modulus (E) (MPa)	Tensile Strength (TS) (MPa)	Strain at break ε (%)	Sol content (%)
P1	n = 5, 4054	0.7 ± 0.1	0.3 ± 0.1	156 ± 23	8.4
P2	n = 10, 5246	1.2 ± 0.1	0.4 ± 0.1	129 ± 11	9.7
P3	n = 20, 7878	12.3 ± 0.5	2.8 ± 0.6	287 ± 11	9.0
SMP1	n = 30, 9859	49.0 ± 1	7.0 ± 1	459 ± 61	6.4
SMP2	n = 40, 11993	47.4 ± 3	10.4 ± 0.3	814 ± 36	8.5

Prepared at conc. = 0.25 g/mol

Representative stress versus strain curves of elastomers prepared at 0.25 g/mL are illustrated in Figure 2.5. The curve shape of semi-crystalline **P3**, **SMP1**, and **SMP2** are noticeably different than that of amorphous **P1** and **P2**. After an initial increase in stress, crystalline lamellae separate into blocks and stress plateaus before another increase is observed due to chains becoming highly orientated. As tensile strength and tensile modulus increased, strain increased with PCL M_n and content due to the reduction in crosslink density. These elastomers systems exhibit deformations greater than other SMP systems.[108, 118] The PCL/PMVS blends as mentioned above, should have provide great flexibility and undergo high percent strains due to the Si-containing segment; however, only 510% was achieved.[99]

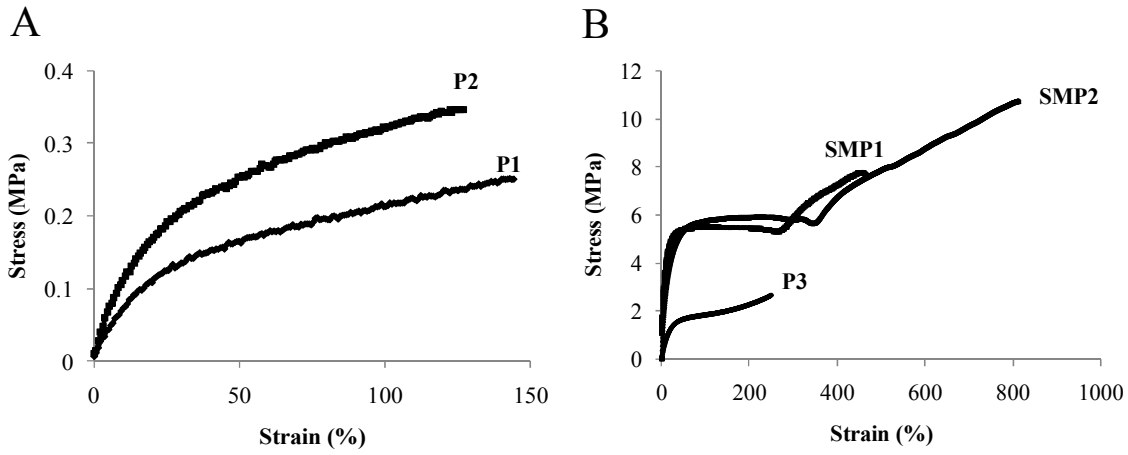

Figure 2.5. Stress vs strain curve of amorphous **P1, P2** elastomers (**A**) and semi-crystalline **P3, SMP1, SMP2** elastomers (**B**). All elastomers prepared at concentration = 0.25 g/mL.

To further modulate mechanical properties we crosslinked **P1**, **P2**, and **SMP1** at three different concentrations (macromer/CH_2Cl_2): 0.25 g/mL, 0.5 g/mL, and 1 g/mL. As macromer concentration was increased, elastomers displayed decreases in percent strain at break with concomitant increase in modulus and tensile strength (Table 2.4, Fig. 2.6). This concentration effect could be explained by closer chain proximity upon photocure at higher concentrations which increases crosslinking efficiency and thereby forms more highly crosslinked systems. This is confirmed by the increased sol content with lower solution concentrations. For networks, as the crosslink density is increased, an increase in modulus and tensile strength and decrease percent strain is expected.

Table 2.4 Effect of concentration on elastomer tensile properties

Elastomer	Concentration (Macromer: DCM)	Tensile Modulus E (MPa)	Tensile Strength T.S. (MPa)	Strain at break ε (%)	Sol content (%)
P1	1:4	0.7 ± 0.1	0.3 ± 0.1	156 ± 23	8.4
	1:2	1.2 ± 0.2	0.3 ± 0.1	39 ± 9	5.4
	1:1	1.6 ± 0.1	0.5 ± 0.1	72 ± 8	3.7
P2	1:4	1.2 ± 0.1	0.4 ± 0.1	129 ± 11	9.7
	1:2	1.4 ± 0.2	0.4 ± 0.1	61 ± 6	5.1
	1:1	1.9 ± 0.4	0.5 ± 0.1	50 ± 3	3.2
SMP1	1:4	49.0 ± 1	7.0 ± 0.1	459 ± 61	6.4
	1:2	34.5 ± 3	7.1 ± 0.6	290 ± 21	5.1
	1:1	31.5 ± 3	6.3 ± 0.2	268 ± 11	3.2

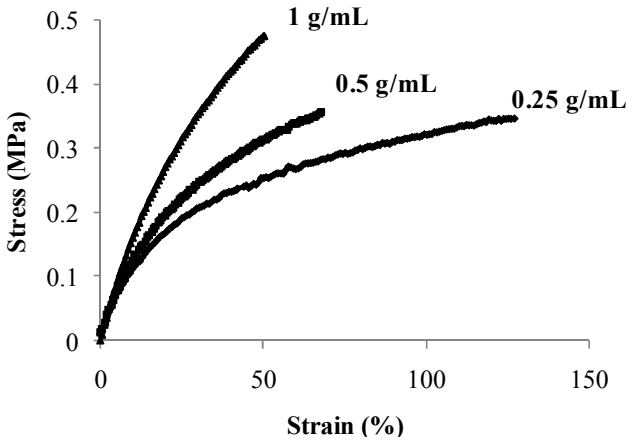

Figure 2.6. Affect of concentration of macromer in CH_2Cl_2 during photochemical cure on mechanical properties of **P2**.

Storage modulus (G') quantifies a material's stiffness or resistance to deformation.[119] Generally, G' increased with increasing PCL block length (Fig. 2.7). For all compositions, G' decreased significantly at ~ -120 °C and ~ -55 °C which corresponds to the T_g of PDMS and PCL respectively. **P1-P3's** storage modulus

becomes undetectable by 0 °C where as **SMP1, SMP2** continue to remain stiff until 60 °C. At 60 °C, crystalline domains melt and remaining mechanical properties are lost.

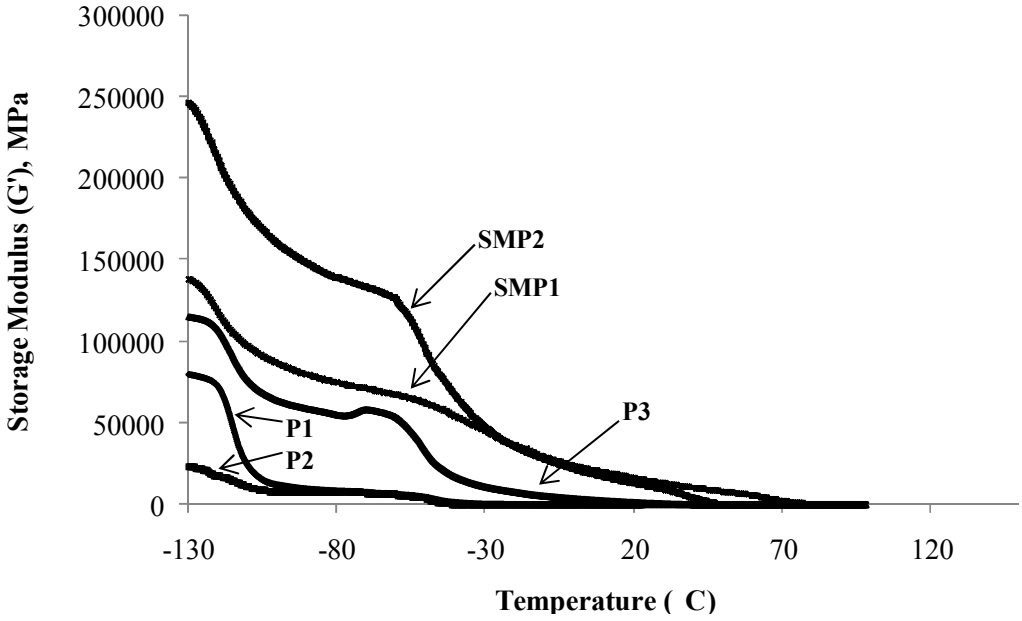

Figure 2.7. Storage Modulus (G') versus temperature (°C). G' increased with increasing PCL block length.

Surface Properties

Water contact angle measurements on elastomer surfaces are reported in Table 2.5. The hydrophobic PDMS control produced a high θ_{static} (15 sec) whereas the θ_{static} of PCL is reported to be lower (~80 – 90 °).[120-122] As expected all elastomers comprised of PDMS and PCL exhibited, static contact angles greater than 90 ° indicating that they are also hydrophobic.[123] Although PCL content systematically increased from 21% (**P1**) to 75% (**SMP2**), no corresponding decrease in the θ_{static} values

closer to that of pure PCL was observed. This may be attributed to the fact that longer PCL segments undergo crystallization which inhibits mobilization to the elastomer-water interface compared to amorphous PCL segments.

Hysteresis ($\theta_\Delta = \theta_{adv} - \theta_{rec}$) is typically used as an indicator of surface reorganization which can occur upon exposure to an aqueous environment.[124] For instance, after wetting a pure silicone surface, polar Si-O-Si groups reorganize to the solid-water interface to minimize interfacial surface tension such that $\theta_{adv} < \theta_{rec}$.[125] For the reported elastomers, reorganization of Si-O-Si groups and PCL segments to the solid-water interface would generate hysteresis. The dynamic contact angle analysis measurements occurred over a 15 sec time period. Somewhat minor hysteresis was observed for all elastomers (θ_Δ = 3-6 °) indicating some surface reorganization. The crosslink density systematically decreases from **P1** to **SMP2** due to the higher M_n of the PCL segments which would favor surface reorganization. However, the crystallinity of longer PCL segments effectively inhibits chain mobilty. Dynamic contact angle analysis was done over a short time period (~15 sec) and thus would only capture rapid surface reorganization. Surface reorganization may be examined during a longer time period (105 sec) by comparing the reduction of θ_{static} (2 min) versus the corresponding θ_{static} (15 sec). For all elastomers, θ_{static} (2 min) was lower than the corresponding θ_{static} (15 sec) from 3-7°. This confirms that reorganization of the elastomers upon exposure to water is not significant, even over longer time periods. Again, this is attributed to either somewhat high crosslink density (**P1-2**) or crystallization of PCL segments (**P3**, **SMP1-2**) which limits mobility of the polymer chains.

Table 2.5 Surface properties of elastomers

Elastomer	Static Contact Angles		Dynamic Contact Angles	
	θ_{static} (°) @ 15 sec	θ_{static} (°) @ 2 min	θ_{adv} (°)	θ_{rec} (°)
P1	105 ± 1	98 ± 2	104 ± 1	100 ± 1
P2	112 ± 3	105 ± 4	111 ± 2	108 ± 3
P3	104 ± 1	102 ± 1	103 ± 1	97 ± 1
SMP1	97 ± 1	95 ± 1	98 ± 1	94 ± 1
SMP2	101 ± 1	97 ± 1	106 ± 1	100 ± 1
Silicone[a]	116 ± 1	115 ± 1	121 ± 1	115 ± 1

[a]**Unmodified Silicone Control** = Dow corning Silastic T-2 cured on a glass microscope slide.
Pure PCL: θ_{static} (°) = 80 – 90 °[120-122]

Thermal Stability

The thermal stability of all acrylated macromers (Fig. 2.8) and the corresponding crosslinked elastomers (Fig. 2.9) were measured in both air and N_2. As expected, acrylated macromers and elastomers began degradation at lower temperatures in air than N_2. Uncrosslinked macromers PDMS (3,000 g/mol) and PCL (2,000 g/mol) served as "high" and "low" thermal stability thermoplastic controls, respectively (Fig. 2.8).

Polysiloxanes display exceptional thermal stability compared to many organic polymers[126] Thus, as a purely organic polymer, the PCL control exhibited significantly lower thermal stability versus the PDMS control. All macromers exhibited enhanced thermal stability compared to the PCL control due to the presence of PDMS segments. All macromers began to degrade at ~315 °C (in N_2) and at ~275 °C (in air) and their final weight was reached by ~ 525 and 600 °C, respectively. Weight loss was slower for macromers with lower % PCL content, particularly **b-p1** (21%) and **b-p2** (35%). Degradation of polysiloxanes in air produces silica residue.[126] Thus, the residue weight produced in air was highest for **b-p1** (~20 %). Crosslinking of macromers was expected to enhance the thermal stability of the corresponding elastomers. However, only minor increases were observed. This may be attributed to macromers undergoing thermally-driven crosslinking prior to the unset of degradation which enhances their thermal stability.

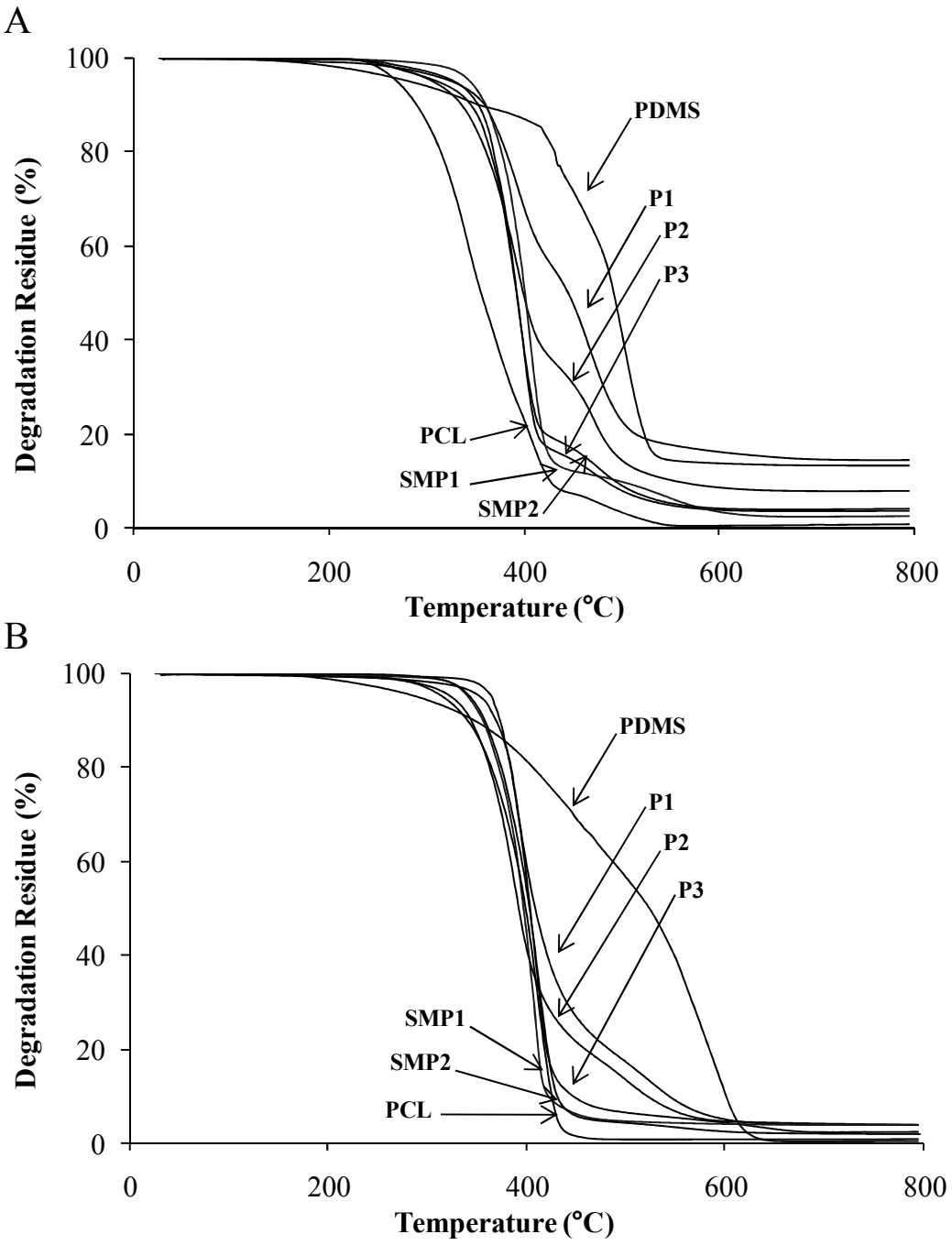

Figure 2.8. Thermal stability of uncrosslinked macromer in air **(A)** and in N_2 **(B).**

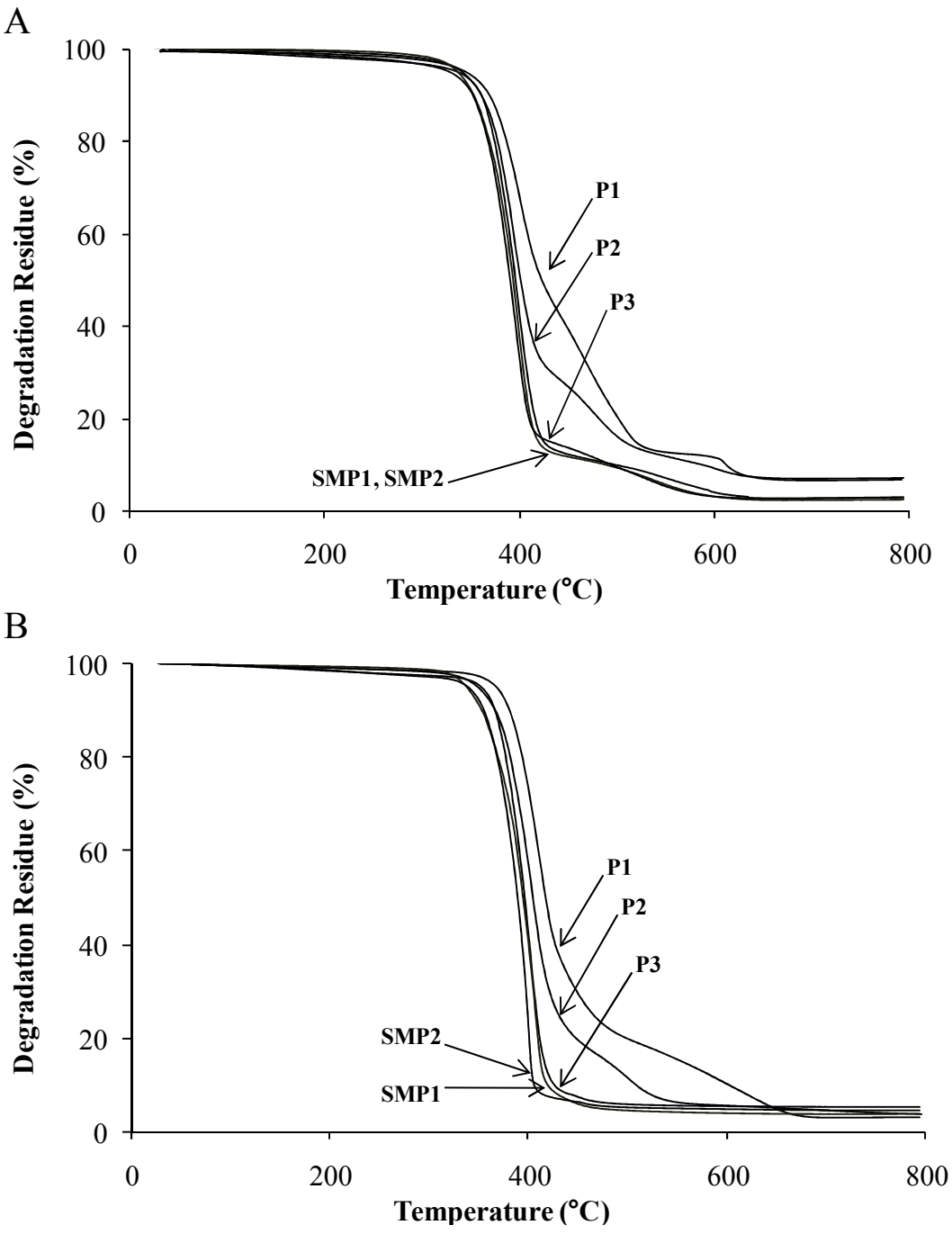

Figure 2.9. Thermal stability of crosslinked elastomer in air **(A)** and in N_2 **(B).**

Shape Memory Properties

Shape memory properties of **SMP1** and **SMP2** were measured via cyclical thermal mechanical tests over four cycles (N) (Fig. 2.10) and strain fixity (R_f), strain recovery rate (R_r) (per equation 2), and total strain recovery rate ($R_{r,tot}$) (per equation 3) were calculated (Table 2.6). The ideal value of R_f, R_r, and $R_{r,tot}$ are 100%.

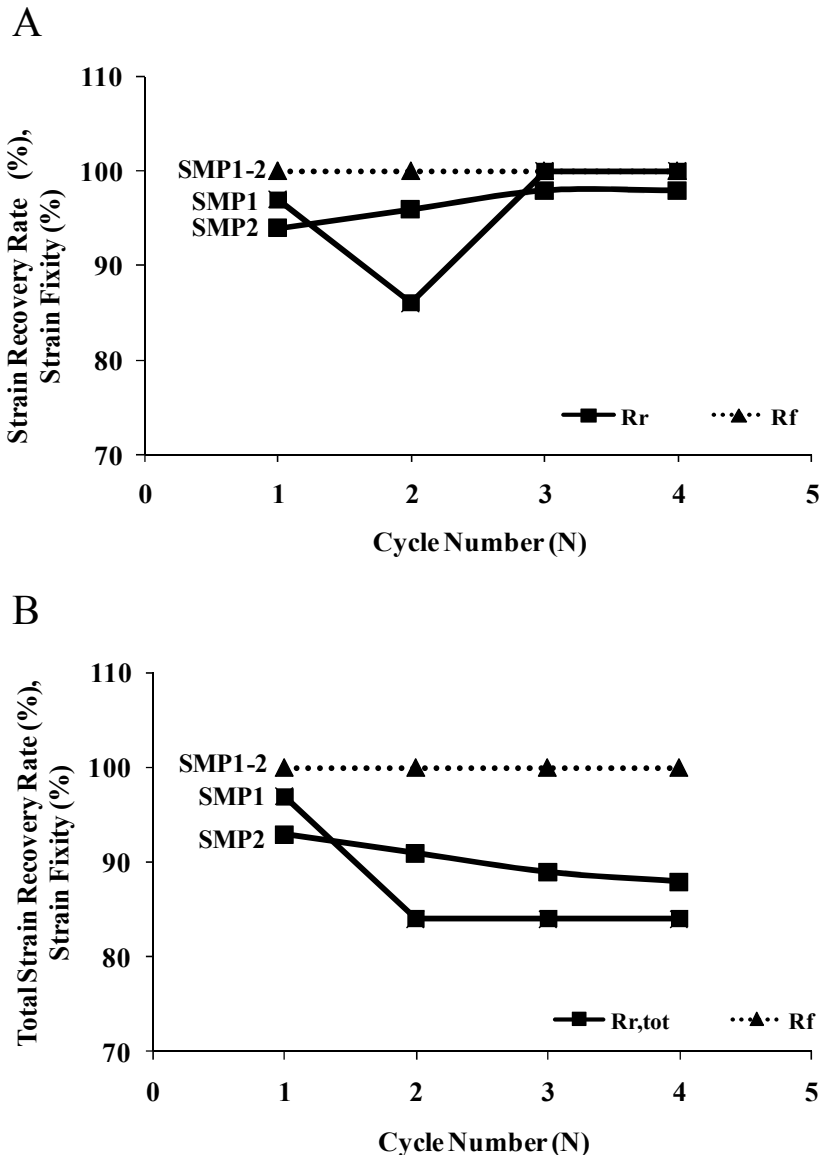

Figure 2.10. (**A, B**) Strain fixity (R_f) versus cycle number and **(A)** strain recovery rate (R_r) versus cycle number and **(B)** total strain recovery rate ($R_{r,tot}$) versus cycle number.

Table 2.6 Shape memory properties

Elastomer	Cycle Number (N)	R_r or "Cycle Dependent"	$R_{r,tot}$ or "Cycle Independent"	R_f
SMP1	1	97	98	100
	2	86	84	100
	3	100	84	100
	4	100	84	100
SMP2	1	94	93	100
	2	96	91	100
	3	98	89	100
	4	98	88	100

Prepared at conc. = 0.25 g/mL

SMP1 and **SMP2** exhibited a shape memory effect whereas **P1-P3** did not. PCL segments which can undergo a melting transition ($T_m = T_{trans}$) may serve as the switching segment. However, the PCL block length of **P1** (n = 5) and **P2** (n = 10) was insufficient for crystallization as confirmed by DSC (Figure 2.3A). PCL block length of **P3** (n = 20) was sufficient to permit nominal crystallization (1.7%) but was insufficient to produce a shape memory effect. However, the PCL segments of **SMP1** (n = 30) and **SMP2** (n = 40) were of sufficient length to permit significant recystallization (29 and 26%, respectively).

For **SMP1** and **SMP2, R_f** was ~100% after each cycle indicating a near perfect ability to memorize the temporary deformed shape (Fig. 2.10). This value is an improvement to PCL-based shape memory systems which exhibited **R_f** values from 86 – 95%.[90, 92, 94, 108, 118] SMPs prepared from the radiation cure of PCL and PMVS blends achieved R_f = 100% value.[99] Total strain recovery rates (**$R_{r,tot}$**) for **SMP1** and **SMP2** ranged from 84 – 98% and 88 – 93%, respectively. **SMP1** and **SMP2** also exhibited a

small decrease in $\mathbf{R_{r,tot}}$ after the first cycle (N =1) (14% and 2%, respectively) (Fig. 2.10B). A slight decrease in $\mathbf{R_{r,tot}}$ from N = 1 to N = 2 is typically observed for SMPs and may be due to extensive chain alignment after the first cycle which prohibits full recovery.[92, 108] $\mathbf{R_{r,tot}}$ of similar PCL based shape memory systems were 93 – 98% and reported as low as 70%.[90, 92, 118] After two cycles strain recovery ($\mathbf{R_r}$) rates were 100% for **SMP1** and 98% for **SMP2,** indicating nearly complete recovery of permanent shape. The slightly improved recovery of **SMP2** may be attributed to its lower crosslink density which enables PCL blocks to more effectively "switch" to a mobile state at $T > T_{trans}$. $\mathbf{R_r}$ values of 99 – 100% after two cycles has been reported for similar PCL bases shape memory systems.[90, 99, 118]

Transition Time

Time series photographs were taken to observe length of time to transition from temporary to permanent shape at 40, 50, and 60 °C in water and in air. Samples were heated, stretched to 150% around cylindrical rod, and quickly cooled to form "coils."

Table 2.7 Transition time from temporary to permanent

Elastomer	Temperature	Time	
		In Air	In Water
SMP1	40 °C	120 s *	30 s *
	50 °C	50 s	8 s
	60 °C	35 s	2 s
SMP2	40 °C	120 s **	120 s **
	50 °C	80 s *	15 s *
	60 °C	45 s	3.5 s

* Partial recovery
** No recovery

All recovery times and indicators for incomplete recovery can be found in Table 2.7. **SMP1** exhibited faster recovery times than **SMP2**. Since both shape memory polymers are stretched to 150%, a quicker recovery time for **SMP1** can be attributed to the higher crosslink density of **SMP1** which creates a higher state of stress in the deformed state which prompts a faster recovery. At a temperature of 67 °C, thermal damage of arterial tissue occurs within a few minutes.[127, 128] Recovery time was quite rapid for both polymers at 60 °C. **SMP1** recovery was 2 sec in water (Fig. 2.11) and 35 sec in air while **SMP2** recovery was 3.5 sec in water and 45 sec in air; therefore, either SMP could be successfully deployed in the body without collateral damage to surrounding tissue. Even if 60 °C was a concern, **SMP1** demonstrated excellent recovery time at 50 °C. As temperature decreased, recovery time was longer and in some instances recovery was partial or none at all. The recovery times for our SMP elastomers are similar and in some instances faster than other shape memory systems.[90, 93, 94, 118, 129]

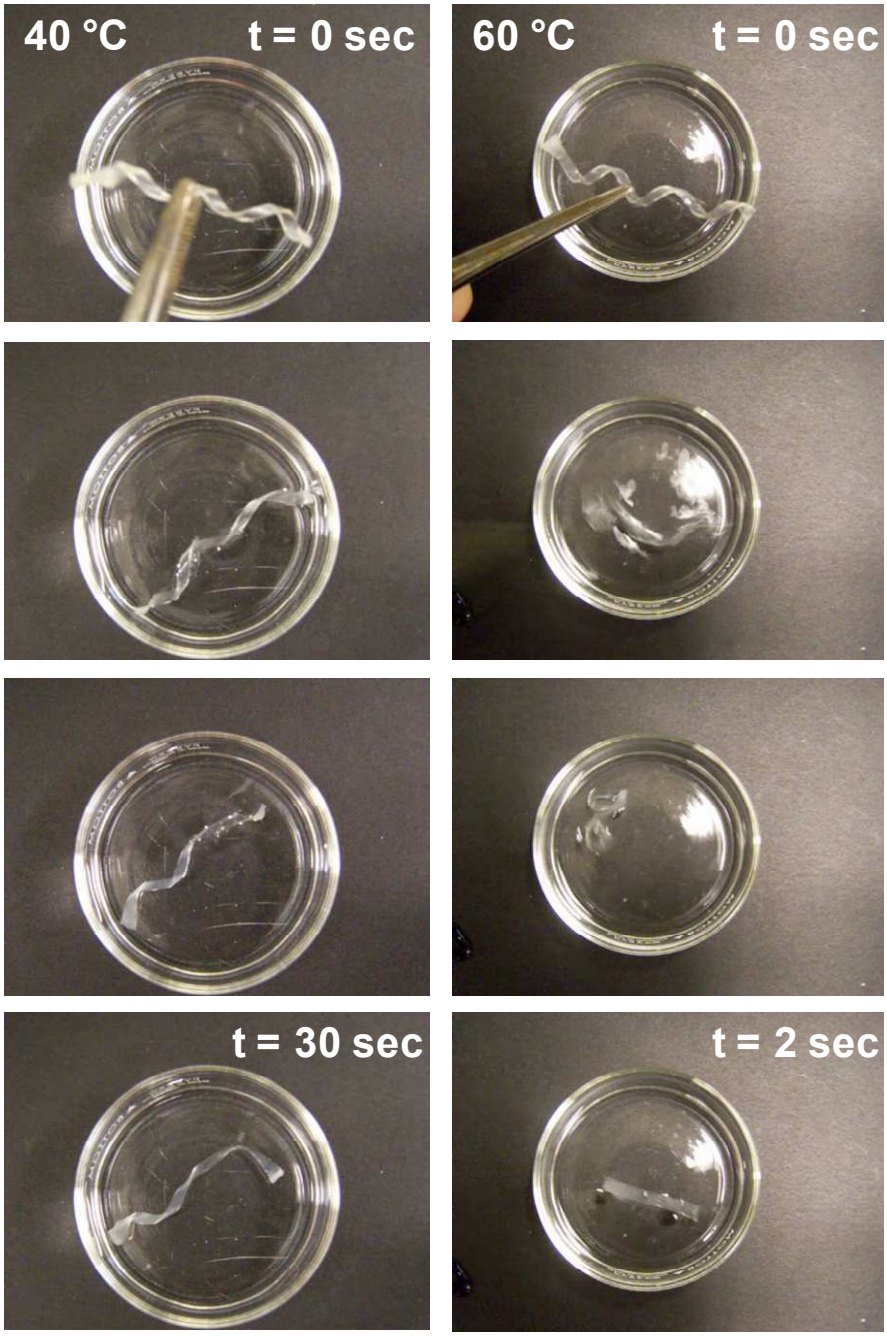

Figure 2.11. Photoseries of transition from temporary to permanent. (**Left**) Elastomer did not fully recovery at 30 sec in 40 °C water. (**Right**) Elastomer fully recovers at 2 sec in 60 °C water.

2.7 Conclusions

Novel, hybrid biodegradable elastomers of the general form PCL_n-*block*-$PDMS_{37}$-*block*-PCL_n have been developed. PDMS, an inorganic polymer, is thermally stable, biocompatible, and exhibits large, recoverable elastic deformation upon crosslinking. PCL is biocompatible, degradable, and also capable of undergoing large deformations. The combination of these two polymers created a unique set of properties suitable for both soft tissue engineering and shape memory bioapplications. Five unique elastomers were synthesized with focus on systematic control of PCL block length while maintaining PDMS block length. By controlling PCL content (i.e. block length) we have demonstrated an ability to modulate and vary mechanical and shape memory properties while sustaining high thermal stability and hydrophobic surfaces (all elastomers > 90 °C). As expected, all elastomers exhibited low T_g's. As PCL block length increased, elastomers began to display crystallinity and once a value greater than 25% crystallinity was met, shape memory properties were exhibited. For both shape memory compositions (**SMP1, SMP2**), strain recovery was > 98% by the third cycle and strain fixity was 100% for all cycles. **SMP1** and **SMP2** also recovered from temporary shape to permanent shape as quick as 2 sec in 60 °C water. Mechanical properties were not only modulated by elastomers composition, but also through concentration upon crosslinking. Therefore, a wide range of customizable mechanical properties have been illustrated: tensile modulus (**E**) 0.72 – 49 MPa, tensile strength (T.S.) 0.25 – 10.4 MPa, and percent strain (**ε**) from 39 – 814%. Customizing biodegradable elastomers mechanical properties could be beneficial, especially for correlating scaffold properties to endpoint engineered

tissue properties. The influence of PCL block length greatly alters polymer properties, but can be used to create a set of biodegradable elastomers for applications in both soft tissue engineering and shape memory polymer settings.

CHAPTER III

BIODEGRADABLE SILICON-CONTAINING ELASTOMERS FOR SOFT TISSUE ENGINEERING SCAFFOLDS AND SHAPE MEMORY FOAMS

3.1 Introduction

The induction of porosity to biodegradable elastomers can permit their utility as tissue engineering scaffolds. In tissue engineering, scaffold porosity provides a highway for the diffusion of nutrients and cellular waste. A variety of methods have been reported to prepare porous polymeric materials including phase separation, gas foaming, emulsion freeze-drying, rapid prototyping techniques, and solvent-casting and salt leaching.[59-62] In addition, a new photolithography technique has been utilized to develop unique micro-patterned systems from photopolymerizable polymers which can be used to control cell response such as cell alignment and expansion.[130-135]

Similarly, introduction of porosity to biodegradable elastomeric shape memory polymers (SMPs) can allow the fabrication of shape memory foams. Techniques used to form porous tissue engineering scaffolds may similarly be used to form foams. Shape memory foams are also highly permeable to air thus reducing the time necessary to transition from temporary to permanent shape.[136] Shape memory foams have become popular in the fields of automotives[137] and heat insulation/energy absorbtion.[138, 139] Shape memory foams are of interest to allow minimally invasive surgical implantation of bulky devices. For instance, shape memory foams have recently been studied for preventing the rupture of aneurysms.[128, 140] In this way, shape memory foams maybe

deployed in the collapsed (temporary) state into some void or defect in the human body and switch to the expanded (permanent) shape upon warming to fill the space. The porous foam in the expanded state acts as a conduit for cell migration, blood flow, nutrients influx, and waste disposal can improve patient comfort and healing time. Shape memory foams fabricated from biodegradable polymers would eliminate surgical intervention to remove the device or eliminate the problems associated with long-term implants.

In the proposed research, porosity was introduced to the biodegradable elastomers synthesized in Chapter II using a porogen-salt leaching technique. Photo-sensitive macromers AcO-PCL_n-*block*-$PDMS_{37}$-*block*-PCL_n-OAc (**b-P1**, **b-SMP1**) were photo-crosslinked in the presence of poly(ethylene glycol) (PEG) and NaCl salts. PEG served as a suspension agent in which NaCl salts can become uniformly dispersed.[141] The PEG and NaCl salts were subsequently leached out of the elastomers thereby producing porous elastomers. The resulting porous, elastomeric scaffolds may be useful as scaffolds for TE scaffolds or shape memory foams.

3.2 Materials

2,2-Dimethoxy-2-phenyl-acetophenone (DMAP), 1-vinyl-2-pyrrolidinone (NVP), poly(ethylene glycol) (PEG; M_n = 2,000), analytical grade salt (250 – 450 μm by sieving. Sieving uses wire mesh to separate salt crystals into specific sizes.), and solvents were obtained from Sigma Aldrich.

3.3 Synthesis Approach

Acrylated macromers AcO-PCL$_n$-*block*-PDMS$_{37}$-*block*-PCL$_n$-OAc (**b-p1;** n=5 and **b-smp;** n = 30) were prepared as described in Chapter II.

3.4 Preparation of Tissue Engineering Scaffolds and Shape Memory Foams

The photosensitive macromers (**b-p1, b-smp1**) were photochemically crosslinked in the presence of poly(ethylene glycol) (PEG) and analytical grade salt (NaCl) using a photoinitiator consisting of 10 wt% solution of DMAP in NVP to create porous analogues (**P1-5, SMP1-5, SMP1-15**). In a typical procedure, the macromer (0.1 g; **b-p1** or **b-smp1**), and PEG (0.608 g) were crushed using a pastel and mortar to a fine powder. The mixture was then transferred to a sealed vial (15 x 48 mm) and dissolved in 425 μL of dichloromethane. The vial was gently shaken by hand or slowly vortexed to completely dissolve PEG and macromer. Next, salt (0.913 g; 250 – 425 μm) and 45μL of photoinitiator solution was added to the vial. After gently vortexing for 15 sec to uniformly distribute salt crystals throughout precursor solution, the vial was quickly exposed to a UV-light (UV-Transilluminator, 6 mW/cm^2, 365 nm) equipped with a foil lined reflection chamber for 3 min. The resulting solvent swollen "plug" was air dried overnight in the open vial. The plug was carefully removed from the vial, placed in 20 mL of 50:50 water to ethanol mixture, and placed on a shaker table for 3 days to remove the PEG and NaCl. The soaking mixture was replaced daily. Three days of soaking produced the expected weight loss based on porogen content. Finally, porous

elastomers were air dried overnight and dried *in vacuo* (36" Hg, 80 °C, 4 h) to remove residual solvent.

3.5 Characterization of Tissue Engineered Scaffolds and Shape Memory Foams

Imaging

Porous elastomer samples were exposed to ruthenium tetroxide vapors to increase conductivity and stability of polymer under electron bombardment. Briefly, 0.02 g of ruthenium chloride was mixed with 1 mL of 10 v/v% sodium hypochlorite to create ruthenium tetroxide vapors which were trapped in a closed glass petri dish with the samples for 10 minutes. To dry, samples were plunged in liquid nitrogen for 30 sec followed by plunging in absolute methanol then hexamethyldisilizane for 20 sec each. Samples were placed on carbon tape covered aluminium specimen stubs and coated with 4 nm of Pt/Pd (80/20) using a Cressington 208HR sputter coater. Images were captured using JOEL JSM-6400 SEM operated at 15kV, 1 nA probe current, and 13 mm working distance or FEI Quanta 600 FE-SEM operated at 10 kV, 130 pA probe current, and 10 mm working distance.

3.6 Results and Discussion

In Chapter II, it was shown that acrylated macromers AcO-PCL_n-*block*-$PDMS_{37}$-*block*-PCL_n-OAc (**b-p1;** n=5 and **b-smp;** n = 30) may be photocrosslinked to form elastomers. It was observed that elastomers prepared from **b-p1** did not exhibit a shape memory effect whereas those prepared from **b-smp1** did. Thus, porous elastomers were

prepared from **b-p1** and **b-smp1** which may be useful as a tissue engineering scaffold and shape memory foam, respectively. However, porous elastomers formed from **b-smp1** may also be useful as a tissue engineering scaffold. Porosity was introduced by using a porogen-salt leaching technique. Macromers were crosslinked in the presence of two porogens: PEG (2k g/mol) and salt (250 – 425 μm). Porogens were subsequently removed by soaking the elastomers in a mixture of water and ethanol for three days. Porogen ratio of salt to PEG was maintained 60:40 wt ratio. By controlling the ratio of macromer to porogens upon crosslinking, porosity was altered. Two different ratios of macromer to porogens were used (Table 3.1) for **b-SMP1** and only one for **b-p1**.

Table 3.1 Porous elastomers notation and ratios of porogen and elastomers

Elastomer	Macromer:Porogen	Porogen Ratio Salt:PEG	Solvent (DCM)	Weight		
				Macromer	PEG	Salt
P1-5	5:95	60:40	425 μL	0.1 g	0.61 g	0.91 g
SMP1-5	5:95	60:40	425 μL	0.1 g	0.61 g	0.91 g
SMP1-15	15:85	60:40	475 μL	0.24 g	0.54 g	0.82 g

P1-5, SMP1-5, and **SMP1-15** were distinctly different in terms of size, shape, and stiffness. The **P1-5** scaffold was significantly more fragile to the touch than either **SMP1-5** or **SMP1-15** foam. These observations parallel the mechanical properties observed in non-porous analogues (Chapter II, Table 2.3). The greater rigidity and strength of **SMP1-5** and **SMP1-15** compared to **P1-5** is attributed to enhanced crystallinity. Also, because **SMP1-15** was prepared with a higher concentration of **b-**

SMP1 macromer, it was stiffer, more expanded, and maintained the cylindrical shape of the "plug" compared to **SMP1-5**. As expected, only **SMP1-5** and **SMP1-15** exhibited a shape memory effect. Thus, these were capable of being deformed to a temporary "compressed" state and then returning to its permanent "expanded" state (Fig. 3.1). A simple experiment to test the expansion of shape memory foam was conducted. An **SMP1-15** "plug" was heated above 70 °C, sandwiched between glass microscope slides, and plunged into an ice bath to lock in temporary "compressed" shape (2.8 mm thick) (Fig. 3.1). The plug was heated back to 70 °C with a heat gun to engage shape memory foam to its permanent "expanded" shape (8.2 mm thick) (Fig. 3.1). In this way, we were able to demonstrate a shape memory foam that is capable of reducing its original size by approximately 200%.

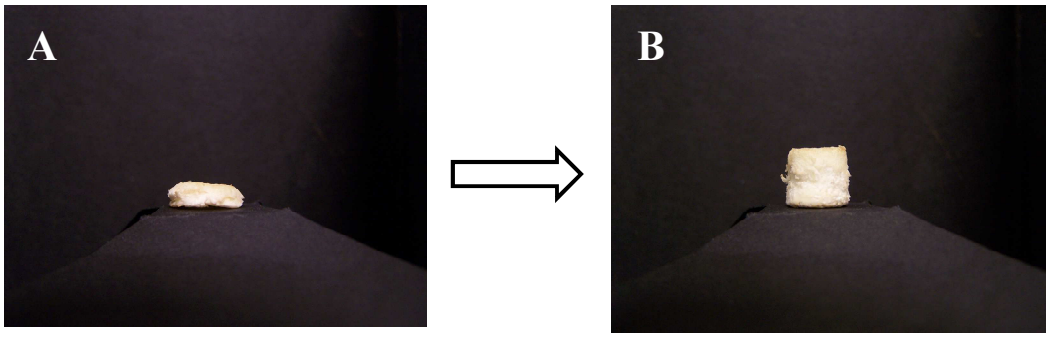

Figure 3.1. Shape memory foams in compressed state (**A**) and expanded state (**B**) of **SMP1-15.**

Imaging

Shape memory foams and biodegradable elastomers were prepped to be conductive and imaged by SEM or FE-SEM. Initial investigations of the **P1-5** foam

revealed both large and small pores created by salt crystals and PEG, respectively (Fig 3.2).

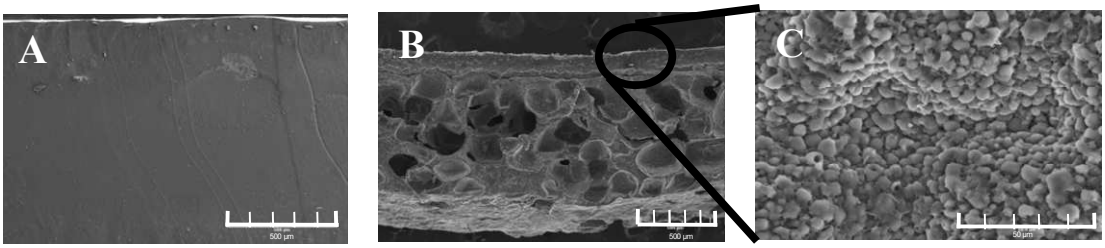

Figure 3.2. Solid elastomers (**A**) of **P1**. Pores created by salt crystals (**B**) and 2k PEG (**C**) of **P1-5**.

SMP1-5 and **SMP1-15** showed similar results as **P1-5**. Since **SMP1-5** and **SMP1-15** demonstrate shape memory properties, FE-SEM images of the "compressed" and "expanded" state were taken and compared (Fig. 3.3). From these images, it is clear that the porous domains of the shape memory foams are being compressed to expel air and take on a temporary "compressed" state. In the expanded state, the pores return to their original size and expand the foam to its original permanent shape.

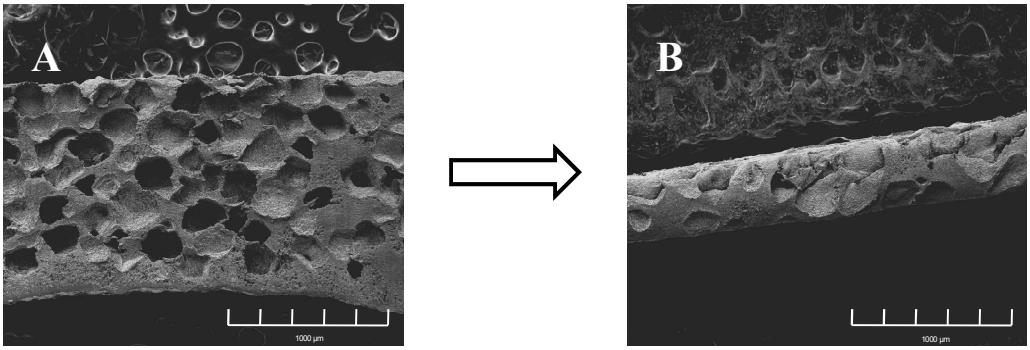

Figure 3.3. FE-SEM images at 100x demonstrated expanded (**A**) and compressed state (**B**) of **SMP1-15**.

3.7 Conclusions

In our initial studies, we demonstrated the ability to introduce porosity to two biodegradable elastomers (**P1-5, SMP1-5, SMP1-15**) using a PEG/salt porogen leaching technique. SEM and FE-SEM imaging demonstrate elastomers with both large and small pores created by salt crystals and PEG, respectively. For **P1-5**, the induction of pores created a scaffold suitable for soft tissue engineering. For **SMP1-5, SMP1-15**, the induction of pores created shape memory foam which could be highly desirable for minimally invasive surgeries. Furthermore, **SMP1-15** illustrated the ability to reduce its size by 200% by collapsing porous domains. Future studies will focus on modifying the porogen leaching technique to induce greater percent porosity such that foams are highly expandable and collapsible.

CHAPTER IV

SUMMARY

In these studies, we developed hybrid biodegradable elastomers comprised of organic and inorganic polymer components in a block copolymer system: poly(ε-caprolactone) (PCL) and poly(dimethylsiloxane) (PDMS), respectively. Tri-block macromers of the form PCL_n-*block*-$PDMS_m$-*block*-PCL_n were developed in which the PDMS block length was maintained (m = 37) and the PCL block length was varied (n = 5, 10, 20, 30, 40). The macromer was capped with acrylating groups (AcO) and formed into elastomers upon exposure to UV light. In this way, variation in crosslink density, PCL content, and PDMS content demonstrated systematic control of resulting thermal, tensile, and shape memory properties. Furthermore, tissue engineered scaffolds and shape memory foams were fabricated by inducing porosity to elastomers.

For all crosslinked biodegradable elastomers, hydrophobic surface properties and high thermal stabilities were exhibited. Elastomers were also highly elastic and reached strains at break as high as 814%. A critical PCL block length (n = 30 or 40) allowed elastomers to exhibit shape memory properties including strain fixity of 100% and strain recovery near 100% after the third thermomechanical cycle. Finally, transition from temporary to permanent shape was rapid (2 sec) and at temperatures near body temperature (60 °C). Shape memory polymers based on an organic-inorganic, photocurable silicon-containing polymer system is a first of its kind and could be valuable for bioapplications.

REFERENCES

1. Tormala, P.; Pohjonen, T.; Rokkanen, P., Bioabsorbable polymers: materials technology and surgical applications. *Proc. Instn. Mech. Engrs.* **1998,** 212, 101-111.

2. Middleton, J.; Tipton, A., Synthetic biodegradable polymers as medical devices. *Medical Plastics and Biomaterials Magazine* 1998.

3. Amsden, B.; Misra, G.; Gu, F.; Younes, H. M., Synthesis and characterization of a photo-cross-linked biodegradable elastomer. *Biomacromolecules* **2004,** 5, (4), 2479-2486.

4. Choi, S.; Park, T. G., Synthesis and characterization of elastic PLGA/PCL/PLGA tri-block copolymers. *J. Biomater. Sci., Polym. Ed.* **2002,** 13, 1163-1173.

5. Coombes, A.; Rizzi, S.; Williamson, M.; Barralet, J.; Downes, S.; Wallace, W., Precipitation casting of polycaprolactone for applications in tissue engineering and drug delivery. *Biomaterials* **2004,** 25, (2), 315-325.

6. Den Dunnen, W. F.; Schakenraad, J. M.; Zondervan, G. J.; Pennings, A. J.; Van Der Lei, B.; Robinson, P. H., A new PLLA/PCL copolymer for nerve regeneration. *J. Mater. Sci: Mater. Med.* **1993,** 4, (5), 521-525.

7. Lee, S.-H.; Kim, B.-S.; Kim, S. H.; Choi, S. W.; Jeong, S. I.; Kwon, I. K.; Kang, S. W.; Nikolovski, J.; Mooney, D.; Han, Y.-K.; Kim, Y. H., Elastic biodegradable poly(glycolide-*co*-caprolactone) scaffold for tissue engineering. *J. Biomed. Mater. Res., Part A* **2003,** 66A, (1), 29-37.

8. Wang, Y.; Ameer, G. A.; Sheppard, B.; Langer, R., A tough biodegradable elastomer. *Nat. Biotechnol.* **2002,** 20, 602-606.

9. Amsden, B.; Tse, M. Y.; Turner, N. D.; Knight, D. K.; Pang, S. C., In vivo degradation behavior of photo-cross-linked *star*-poly(epsilon-caprolactone-*co*-D,L-lactide) elastomers. *Biomacromolecules* **2006,** 7, (1), 365-372.

10. Chan-Park, M. B.; Zhu, A. P.; Shen, J. Y.; Fan, A. L., Novel photopolymerizable biodegradable triblock polymers for tissue engineering scaffolds: synthesis and characterization. *Macromol. Biosci.* **2004,** 4, (7), 665-673.

11. Grijpma, D. W.; Hou, Q.; Feijen, J., Preparation of biodegradable networks by photo-crosslinking lactide, ε-caprolactone, and trimethylene carbonate-based oligomers functionalized with fumaric acid monoethyl ester. *Biomaterials* **2005,** 26, (16), 2795-2802.

12. Helminen, A. O.; Korhonen, H.; Seppala, J. V., Cross-linked poly(epsilon-caprolactone/D,L-lactide) copolymers with elastic properties. *Macromol. Chem. Phys.* **2002,** 203, (18), 2630-2639.

13. Griffith, L. G.; Naughton, G., Tissue engineering - current challenges and expanding opportunities. *Science* **2002,** 295, 1009-1014.

14. Sweigart, M. A.; Athanasiou, K. A., Towards tissue engineering of the knee meniscus. *Tissue Engr.* **2001,** 7, 111-129.

15. Callister, W. D., *Fundamentals of Materials Science and Engineering*. 2nd ed.; John Wiley & Sons, Inc.: Hoboken, NJ, 2005.

16. Groot, J. H. d.; Spaans, C. J.; Dekens, F. G.; Pennings, A. J., On the role of aminolysis and transesterification in the synthesis of e-caprolactone and L-lactide based polyurethanes. *Polym. Bull.* **1998,** 41, 299-306.

17. Kylma, J.; Seppala, J. V., Synthesis and characterization of a biodegradable thermoplastic poly(ester-urethane) elastomer. *Macromolecules* **1997,** 30, 2876-2882.

18. Baez, J. E.; Marcos-Fernandez, A.; Lebron-Aguilar, R.; Martinez-Richa, A., A novel route to a,w-telechelic poly(e-caprolactone) diols, precursors to biodegradable polyurethanes, using catalysis by decamolybdate anion. *Polymer* **2006,** 47, 8420-8429.

19. Yeganeh, H.; Jamshidi, H.; Jamshidi, S., Synthesis and properties of novel biodegradable poly(e-caprolacone)/poly(ethylene glycol)-based polyurethane elastomers. *Polym. Int.* **2007,** 56, 41-49.

20. Sipos, L.; Zsuga, M.; Deak, G., Synthesis of poly(L-lactide)-block-polyisobutylene-block-poly(L-lactide), a new biodegradable thermoplastic elastomer. *Macromol. Rapid Commun.* **1995,** 16, 935-940.

21. Yang, J.; Webb, A. R.; Ameer, G. A., Novel citric acid-based biodegradable elastomers for tissue engineering. *Adv. Mater.* **2004,** 16, 511-516.

22. Yang, J.; Motlagh, D.; Webb, A. R.; Ameer, G. A., Novel biphasic elastomeric scaffold for small-diameter blood vessel tissue engineering. *Tissue Eng.* **2005,** 11, 1876-1886.

23. Yang, J.; Webb, A. R.; Pickerill, S. J.; Hageman, G.; Ameer, G. A., Synthesis and evaluation of poly(diol citrate) biodegradable elastomers. *Biomaterials* **2006,** 27, 1889-1898.

24. Kang, Y.; Yang, J.; Khan, S.; Anissian, L.; Ameer, G. A., A new biodegradable polyester elastomer for cartilage tissue engineering. *J. Biomed. Mater. Res.* **2006,** 77A, 331-339.

25. Webb, A. R.; Kumar, V. A.; Ameer, G. A., Biodegradable poly(diol citrate) nanocomposite elastomers for soft tissue engineering. *J. Mater. Chem.* **2007,** 17, 900-906.

26. Lee, S.-H.; Kim, B.-S.; Kim, S. H.; Choi, S. W.; Jeong, S. I.; Kwon, I. K.; Kang, S. W.; Nikolovski, J.; Mooney, D. J.; Han, Y.-K.; Kim, Y. H., Elastic biodegradable poly(glycolide-*co*-caprolactone) scaffold for tissue engineering. *J. Biomed. Mater. Res.* **2003,** 66A, 29-37.

27. Martin, D. P.; Williams, S. F., Medical applications of poly-4-hydroxybutyrate: a strong flexible absorbable biomaterial. *J. Biochem. Eng.* **2003,** 16, 97-105.

28. Misra, S. K.; Valappil, S. P.; Roy, I.; Boccaccini, A. R., Polyhydroxyalkanoate (PHA)/inorganic phase composites for tissue engineering applications. *Biomacromolecules* **2006,** 7, 2249-2258.

29. Palmgren, R.; Karlsson, S.; Albertsson, A.-C., Synthesis of degradable crosslinked polymers based on 1,5-dioxepan-2-one and crosslinker of bis-e-caprolactone type. *J. Polymer. Sci. Part A: Polym. Chem.* **1997,** 35, 1635-1649.

30. Turunen, M. P.; Korhonen, H.; Tuominen, J.; Seppala, J. V., Synthesis, characterization and crosslinking of functional star-shaped poly(e-caprolactone). *Polym. Int.* **2001,** 51, 92-100.

31. Storey, R. F.; Warren, S. C.; Allison, C. J.; Wiggins, J. S.; Puckett, A. D., Synthesis of bioabsorbable networks from methacrylate-endcapped polyesters. *Polymer* **1993,** 34, 4365-4372.

32. Allcock, H. R.; McDonnell, G. S.; Desorcie, J. L., Synthesis of new polyphosphazene elastomers. *Macromolecules* **1990,** 23, 3873-3877.

33. Allcock, H. R., Cross-linking reactions for the conversion of polyphosphazenes into useful materials. *Chem. Mater.* **1994,** 6, 1476-1491.

34. Wang, Y.; Ameer, G. A.; Sheppard, B. J.; Langer, R., A tough biodegradable elastomer. *Nat. Biotechnol.* **2002,** 20, 602-606.

35. Motlagh, D.; Yang, J.; Lui, K. Y.; Webb, A. R.; Ameer, G. A., Hemocompatibility evaluation of poly(glycerol-sebacate) in vitro for vascular tissue engineering. *Biomaterials* **2006,** 27, 4315-4324.

36. Amsden, B. G.; Misra, G.; Gu, F.; Younes, H. M., Synthesis and characterization of a photo-cross-linked biodegradable elastomer. *Biomacromolecules* **2004,** 5, 2479-2486.

37. Amsden, B. G.; Tse, M. Y.; Turner, N. D.; Knight, D. K.; Pang, S. C., In vivo degradation behavior of photo-cross-linked *star*-poly(ε-caprolactone-*co*-D,L-lactice) elastomers. *Biomacromolecules* **2006,** 7, 365-372.

38. Nijst, C.; Bruggeman, J.; Karp, J.; Ferreira, L.; Zumbuehl, A.; Bettinger, C.; Langer, R., Synthesis and characterization of photocurable elastomers from poly(glycerol-co-sebacate). *Biomacromolecules* **2007,** 8, 3067-3073.

39. Grego, A. V.; Mingrone, G., Dicarboxylic acids, an alternative fuel substrate in parenteral nutrition: an update. *Clinical Nutr.* **1995,** 14, (3), 143-148.

40. Yang, J.; Webb, A. R.; Ameer, G. A., Novel citric acid-based biodegradable elastomers for tissue engineering. *Adv. Mat.* **2004,** 16, (6), 511-516.

41. Butler, D. L.; Kay, M. D.; Stouffer, D. C., Comparison of material properties in fascicle-bone units from human patellar tendon and knee ligaments. *J. Biomech.* **1986,** 19, (6), 425-432.

42. Chandran, K. B., *Cardiovascular Mechanics*. 1 ed.; New York University Press: New York, 1992; p 300.

43. Gupta, B. S.; Kasyanov, V. A., Biomechanics of human common carotid artery and design of novel hybrid textile compliant vascular grafts. *J. Biomed. Mater. Res.* **1997,** 34, (3), 341-349.

44. Johnson, G. A.; Tramaglini, D. M.; Levine, R. E.; Ohno, K.; Choi, N.-Y.; Woo, S. L.-Y., Tensile and viscoelastic properties of human patellar tendon. *J. Bone and Joint Surg.* **1994,** 12, (6), 796-803.

45. Lee, J. M.; Boughner, D. R., Mechanical properties of human pericardium. *Circul. Res.* **1985,** 57, (3), 475-481.

46. Martin, D. P.; Williams, S. F., Medical applications of poly-4-hydroxybutyrate: a strong flexible absorbable biomaterial. *J. Biochem. Engr.* **2003,** 16, (2), 97-105.

47. Yang, S.; Leong, K.-F.; Du, Z.; Chee-Kai, The design of scaffolds for use in tissue engineering. Part I. Traditional factors. *Tissue Engr.* **2001,** 7, (6), 679-689.

48. Pitt, C. G.; Gratzl, M. M.; Kimmel, G. L.; Surles, J.; Schindler, A., Aliphatic polyesters II. The degradation of poly(DL-lactide), poly(ϵ-caprolactone), and their copolymers in vivo. . *Biomaterials* **1981,** 2, (4), 215-220.

49. Nagata, M.; Sato, Y., Synthesis and properties of photocurable biodegradable multiblock copolymers based on poly(ε-caprolactone) and poly(l-lactide) segments. *J. Polym. Sci., Part A: Polym. Chem.* **2005,** 43, 2426-2439.

50. Pego, A.; Grijpma, D. W.; Feijen, J., Enchanced mechanical properties of 1,3-trimethylene carbonate polymers and networks. *Polymer* **2003,** 44, 6495-6504.

51. Cohn, D.; Stern, T.; Gonzalez, M. F.; Epstein, J., Biodegradable poly(ethylene oxide)/poly(ε-caprolactone) multiblock copolymers. *J. Biomed. Mater. Res.* **2002,** 59, 273-281.

52. Lodge, T. P., Block copolymers: past successes and future challenges. *Macromol. Chem. Phys.* **2003,** 204, 265-273.

53. Martina, M.; Hutmacher, D. W., Biodegradable polymers applied in tissue engineering research: a review. *Polym. Int.* **2007,** 56, 145-157.

54. Kumar, N.; Ravikumar, M. N. V.; Domb, A. J., Biodegradable block copolymers. *Adv. Drug Delivery Rev.* **2001,** 53, 23-44.

55. Boccaccini, A. R.; Maquet, V., Bioresorbable and bioactive polymer/Bioglass composites with tailored pore structure for tissue engineering applications. *Composite Sci. Tech.* **2003,** 63, 2417-2479.

56. Ranucci, C. S.; Kumanr, A.; Batra, S. P.; Moghe, P., Control of hepatocyte function on collagen foams: sizing matrix pores toward selective inductionon of 2-D and 3-D cellular morphologies. *Biomaterials* **2000,** 21, 783-793.

57. Spector, M.; Michno, M. J.; Smarook, W. H.; Kwiakowski, G. T., A high-modulus polymer for porous orthopedic implants: biomechanical compatibility of porous implants. *J. Biomed. Mater. Res.* **1978,** 12, 665-677.

58. Whang, K.; Thomas, C. H.; Healy, K. E., A novel method to fabricate bioabsorbable scaffolds. *Polymer* **1995,** 36, 837-842.

59. Hutchmacher, D. W., Scaffolds for tissue engineering bone and cartilage. *Biomaterials* **2000,** 21, 2529-2543.

60. Argawal, C. M.; Athanasiou, K. A.; Heckman, J. D., Biodegradable PLA-PGA polymers for tissue engineering in orthopedics. *Mat. Sci. Forum* **1997,** 250, 115-128.

61. Yang, S.; Leong, K.-F.; Du, Z.; Chua, C.-K., The design of scaffolds for use in tissue engineering. Part I. Traditional factors. *Tissue Eng.* **2001,** 7, 679-689.

62. Thomas, R. C.; Yaszemski, M. J.; Mikos, A. G., In *Principles of Tissue Engineering*, Lanza, R. P.; Langer, R.; Chick, W. L., Eds. R.G. Landes: Austin, TX, 1997; pp 263-271.

63. Burdick, J.; Frankel, D.; Dernell, W.; Anseth, K., An initial investigation of photocurable three-dimensional lactic acid based scaffolds in a critical-sized cranial defect. *Biomaterials* **2003,** 24, (9), 1613-1620.

64. Yang, Q.; Chen, L.; Shen, X.; Tan, A., Preparation of polycaprolactone tissue engineering scaffolds by improved solvent casting/particulate leaching method. *J. Macro. Sci., Part B: Phys.* **2006,** 45, (6), 1171-1181.

65. Rhodes, N. P.; Bellon, J. M.; Bujan, M. J.; Soldani, G.; Hunt, J. A., Inflammatory response to a novel series of siloxane-crosslinked polyurethane elastomers having controlled biodegradation. *J. Mater. Sci.: Mater. Med.* **2005,** 16, 1207-1211.

66. Rhodes, N. P.; Bellon, J. M.; Bujan, M. J.; Soldani, G.; Hunt, J. A., Inflammatory response to a novel series of siloxane-crosslinked polyurethane elastomers having controlled biodegradation. *J. Mater. Sci: Mater. Med.* **2005,** 16, 1207-1211.

67. Langer, R.; Vacanti, J. P., Tissue engineering. *Science* **1993,** 260, (5110), 920-926.

68. Gunatillake, P. A.; Adhikar, R., Biodegradable synthetic polymers for tissue engineering. *Eur. Cells Mater.* **2003,** 5, 1-16.

69. Nair, L. S.; Laurencin, C. T., Polymers as biomaterials for tissue engineering and controlled drug delivery *Adv. Biochem. Engr. / Biotech.* **2006,** 102, 47-90.

70. Webb, A. R.; Yang, J.; Ameer, G. A., Biodegradable polyester elastomers in tissue engineering. *Expert Opin. Biol. Ther.* **2004,** 4, (6), 801-812.

71. Athanasiou, K. A.; Agrawal, C. M.; Barber, F. A.; Burkhart, S. S., Orthopaedic applications for PLA-PGA biodegradable polymers. *J. Arthro. Rel. Surg.* **1998,** 14, (7), 726-737.

72. Xie, J.; Ihara, M.; Jung, Y.; Kwon, I. K.; Kim, S. H.; Kim, Y. H.; Matsuda, T., Mechano-active scaffold deisgn based on microporous poly(l-lactide-co-ε-caprolactone) for articular cartilage tissue engineering: dependence of porosity on compression force-applied mechanical behaviors. *Tissue Engr.* **2006,** 12, 449-458.

73. Mo, X.; Weber, H. J.; Ramakrishna, S., PCL-PGLA compositve tubular scaffold preparation and biocompatibility investigation. *Internat. J. Artificial Organs* **2006,** 29, 790-799.

74. Lendlein, A.; Kelch, S., Shape-memory polymer. *Angew. Chem. Int. Ed.* **2002,** 41, 2034-2057.

75. Yakacki, C. M.; S., W.; Luders, C.; Gall, K., Deformation limits in shape-memory polymers. *Adv. Eng. Mater.* **2008,** 10, (112-119).

76. Zhu, G.; Liang, G.; Xu, Q.; Yu, Q., Shape-memory effects of radiation crosslinked poly(ε-caprolactone). *J. Appl. Polym. Sci.* **2003,** 90, 1589-1595.

77. Lendlein, A.; Langer, R., Biodegradable, elastic shape-memory polymers for potential biomedical applications. *Science* **2002,** 296, 1673 - 1676.

78. Yakacki, C. M.; Shandas, R.; Lanning, C.; Rech, B.; Eckstein, A.; Gall, K., Unconstrained recovery characterization of shape-memory polymer networks for cardiovascular applications. *Biomaterials* **2007,** 28, 2255-2263.

79. Wache, H. M.; Tartakowska, D. J.; Hentrich, A.; Wagner, M. H., Development of a polymer stent with shape memory effect as a drug delivery system. *J. Mater. Sci.: Mater. Med.* **2003,** 14, 109-112.

80. Gall, K.; Kreiner, P.; Turner, D.; Hulse, M., Shape-memory polymers for microelectromechanical systems. *J. Microelectromech. Syst.* **2004,** 13, 472-483.

81. Doraiswami, R.; Wornyo, E.; Bhattacharya, S.; Gall, K., Shape-memory capacitors for next generation embedded actives. In *Electronic Components and Technology Conference*, 2006; pp 520-522.

82. Liu, G.; Ding, X.; Cao, Y.; Zheng, Z.; Peng, Y., Novel shape-memory polymer with two transition temperatures. *Macromolec. Rapid Commun.* **2005,** 26, 649-652.

83. Liu, G.; Ding, X.; Cao, Y.; Zheng, Z.; Peng, Y., Shape memory of hydrogen-bonded polymer network/poly(ethylene glycol) complexes. *Macromolecules* **2004,** 37, 2228-2232.

84. Ling, J. R.; Chen, L. W., Study on shape-memory behavior of polyether-based polyurethanes. I. Influence of the hard-segment content. *J. Appl. Polym. Sci.* **1998,** 69, 1563-1574.

85. Armani, D. K.; Liu, C., Microfabrication technology for polycaprolactone, a biodegradable polymer. *J. Micromech. Microeng.* **2000,** 10, 80-84.

86. Iojoiu, C.; Hamaide, T.; Harabagiu, V.; Simionescu, B., Modified poly(ε-caprolactone)s and their use for drug-encapsulating nanoparticles. *J Polym Sci Part A: Polym Chem* **2004,** 2004, 689-700.

87. Cao, Q.; Chen, S.; Hu, J.; Liu, P., Study on the liquefied-MDI-based shape memory polyurethanes. *J. Appl. Polym. Sci.* **2007,** 106, 993-1000.

88. Kim, B. K.; Lee, S. Y., Polyurethanes having shape memory effects. *Polymer* **1996,** 26, 5781-5793.

89. Zhuohong, Y.; Jinlian, H.; Yeqiu, L.; Lapyan, Y., The study of crosslinked shape-memory polyurethanes. *Materials Chemistry and Physics* **2006,** 98, 368-372.

90. Lendlein, A.; Schmidt, A.; Langer, R., AB-polymer networks bases on oligo(ε-caprolactone) segments showing shape-memory properties. *PNASs* **2001,** 98, 842 - 847.

91. Lu, X. L.; Cai, W.; Gao, Z. Y., Shape-memory behaviors of biodegradable poly(L-lactide-co-ε-caprolactone) copolymers. *J. Appl. Polym. Sci.* **2008,** 108, 1109-1115.

92. Lu, X. L.; Cai, W.; Zhiyong, G.; Tang, W. J., Shape memory effects on poly(L-lactide) and its copolymer with poly(ε-caprolactone). *Polymer Bulletin* **2007,** 58, 381-391.

93. Lu, X. L.; Sun, Z. J.; Cai, W.; Gao, Z. Y., Study on the shape memory effects of poly(L-lactide-co-ε-caprolactone) biodegradable polymers. *J. Mater. Sci.: Mater. Med.* **2008,** 19, 395 - 399.

94. Min, C.; Cui, W.; Bei, J.; Wang, S., Biodegradable shape-memory polymer-polylactide-co-poly(glycolide-co-caprolactone) multiblock copolymer. *Polym. Adv. Technol.* **2005,** 16, 608-615.

95. Nagata, M.; Kitazima, I., Photocurable biodegradable poly(ε-caprolactone)/poly(ethylene glycol) multiblock copolymers showing shape-memory properties. *Colloid Polym. Sci.* **2006,** 284, 380-386.

96. Curtis, J.; Colas, A., *Medical Applications of Silicones*. 2nd ed.; San Diego, CA, 2004.

97. Dyke, M. E. V.; Clarson, S. J.; Arshady, R., *Silicone Biomaterials*. Vol. 1, Citrus Books: London, 2003.

98. Kayaman-Apohan, N.; Karal-Yilmaz, O.; Baysal, K.; Baysal, B. M., Poly(DL-lactic acid)/triblock PCL-PDMS-PCL copolymers: synthesis, characterization, and demonstration of their cell growth effects in vitro. *Polymer* **2001,** 42, 4109-4116.

99. Zhu, G.; Xu, S.; Wang, J.; Zhang, L., Shape memory behaviour of radiation-crosslinked PCL/PMVS blends. *Radiat. Phys. Chem.* **2006,** 75, 443-448.

100. Bachari, A.; Belorgey, G.; Helary, G.; Sauvet, G., Synthesiis and characterization of multiblock copolymers poly[poly(L-lactide)-block-polydimethylsiloxane]. *Macromol. Chem. Phys.* **1995,** 196, 411-428.

101. Ekin, A.; Webster, D. C., Synthesis and characterization of novel hydroxyalkyl carbamate and dihydroxyalkyl carbamate terminated poly(dimethylsiloxane) oligomers and their block copolymers with poly(ε-caprolactone). *Macromolecules* **2006,** 39, 8659-8668.

102. Lee, W. K., Synthesis of polyester/poly(dimethylsiloxane)/polyester triblock copolymers and their rearrangement under water: rearrangment of PDMS-containing copolymers. *Composite Interfac.* **2006,** 13, 159-171.

103. Porjazoska, A.; Cvetkovska, M.; Yilmaz, O. K.; Baysal, K.; Apohan, N. K.; Baysal, B. M., Synthesis and characterization of biocompatible multicomponent polymer systems as supports for cell cultures. *Bull. Chem. Tech. Macedonia* **2004,** 23, 147-156.

104. Yilgor, I.; Warren P. Steckle, J.; yilgor, E.; Freelin, R. G.; Riffle, J. S., Novel triblock siloxane copolymers: synthesis, characterization, and their use as surface modifying additives. *J. Polymer. Sci. Part A: Polym. Chem.* **1989,** 27, 3673-3690.

105. Du, J. Z.; Sun, T. M.; Weng, S. Q.; Chen, X. S., Wang, J., Synthesis and characterization of photo-cross-linked hydrogels based on biodegradable polyphosphoesters and poly(ethylene glycol) copolymers *Biomacromolecules* **2007,** 8, 3375-3381.

106. Lam, C.; Savalani, M.; Teoh, S.; Hutmacher, D., Dynamics of in vitro polymer degredation of polycaprolactone-based scaffolds: accelerated versus simulated physiolgocial conditions. *Biomed. Mater.* **2008,** 3, 1-15.

107. Toncheva, V.; Bulcke, A.; Schacht, E.; Mergaert, J.; Swings, J., Synthesis and environmental degradation of polyesters based on poly(ε-caprolactone. *J. Environ. Polym. Degrad.* **1996,** 4, 71-83.

108. Rabani, G.; Luftmann, H.; Kraft, A., Synthesis and characterization of two shape-memory polymers containing short aramid hard segments and poly(ε-caprolactone) soft segments. *Polymer* **2006,** 47, 4251-4260.

109. Sperling, L. H., *In Introduction to Physical Polymer Science* 3rd ed.; John Wiley & Sons: New York, 2001.

110. Chandler, L. A.; Collins, E., Multiple glass transitions in butadiene-acrylonitrile copolymers. *J. Appl. Polym. Sci.* **1969,** 13, 1585-1593.

111. Dell'Erba, R.; Groeninckx, B.; Maglio, G.; Malinconico, M.; Migliozzi, A., Immiscible polymer blends of semicyrstalline biocompatible components: thermal properties and phase morphology analysis of PLLA/PCL blends. *Polymer* **2001,** 42, 7831-7840.

112. Deng, X. M.; Xiong, C. D.; Cheng, L. M.; XU, R. P., Synthesis and characterization of block copolymers from D,L-lactide and poly(ethylene glycol) with stannous chloride. *J. Polym. Sci., Part C: Polym. Lett.* **1990,** 28, 411-416.

113. Clarson, S. J.; Semlyen, J. A., *Siloxane Polymers*. Prentice-Hall: Englewood Cliffs, NJ, 1993.

114. Lotters, J. C.; Olthuis, W.; Veltink, P. H.; Bergveld, P., The mechanical properties of the rubber elastic polymer polydimethylsiloxane for sensor applications. *J. Micromech. Microeng.* **1997,** 7, 145-147.

115. Dlubek, G.; Supej, M.; Bondarenko, V.; Pionteck, J.; Pompe, G.; Krause-Rehberg, R.; Emri, I., Ortho-positronium lifetime distribution analyzed with MELT and LT and free volume in poly(ε-caprolactone) during glass transition, melting, and crystallization. *J. Polym. Sci., Part B: Polym. Phys.* **2003,** 41, 3077-3088.

116. Koleske, J. V.; Lundber, R. D., Lactone polymers. I. Glass transition temperature of poly(ε-caprolactone) by means of compatible polymer mixtures. *J. Polym. Sci., Part A: Polym. Chem.* **1969,** 7, 795-807.

117. Zhou, S.; Deng, X.; Yang, H., Biodegradable poly(ε-caprolactone)-poly(ethylene glycol) block copolymers: characterization and their use as drug carriers for controlled delivery system. *Biomaterials* **2003,** 24, 3563-3570.

118. Lendlein, A.; Schmidt, A.; Schroeter, M.; Langer, R., Shape-memory polymer networks from oligo(ε-caprolactone) dimethacrylates. *J. Polym. Sci., Part A: Polym. Chem.* **2005,** 43, 1369 - 1381.

119. Wicks, Z. W.; Jones, F. N.; Pappas, S. P., *Organic Coatings Science and Technology*. 2nd ed.; John Wiley & Sons: New York, 1999.

120. Erbil, H.; Yasar, B.; Suzer, S.; Baysal, B., Surface characterization of the hydroxy-terminated poly(ε-caprolactone)/poly(dimethylsiloxane) triblock copolymers by electron spectroscopy for chemical analysis and contact angle measurements. *Langmuir* **1997,** 13, 5484-5493.

121. Hu, S.; Cao, X.; Song, Y.; Li, C.; Xie, P.; Jiang, L., New responsive property of poly(ε-caprolactone) as the thermal switch from superhydrophobic to superhydrophilic. *Chem. Commun.* **2008**, 2025-2027.

122. Zhu, Y.; Gao, C.; Liu, X.; Shen, J., Surface modification of polycaprolactone membrane via aminolysis and biomacromolecule immobilization for promoting cytocompatibility of human endothelial cells. *Biomacromolecules* **2002,** 3, 1312-1319.

123. Sangermano, M.; Bongiovanni, R.; Malucelli, G.; Priola, A.; Pollicino, A.; Recca, A., Fluorinated epoxides as surface modifying agents of UV-curable systems. *J. Appl. Polym. Sci.* **2003,** 89, 1524-1529.

124. Sui, G.; Wang, J.; Lee, C.-C.; Lee, S. P.; Leyton, J. V., Solution-phase surface modification in intact poly(dimethylsiloxane) microfluidic channels. *Anal. Chem.* **2006,** 78, 5543-5551.

125. Brook, M. A., *Silicon in Organic, Organometallic, and Polymer Chemistry*. John Wiley & Sons, Inc.: New York, NY, 2000.

126. Dvornic, P. R., *Thermal Properties of Polysiloxanes. In Silicon-Containing Polymers*. Kluwer Academic Publishers: Dordrecht, 2000.

127. Agah, R.; Pearce, J. A.; Welch, A. J.; Motamedi, M., Rate process model for arterial tissue thermal damage: implications on vessel photocoagulation. *Lasers Surg. Med.* **1994,** 15, 176-184.

128. Maitland, D.; Small, W.; Ortega, J.; Buckley, P.; Rodriguez, J.; Hartman, J.; Wilson, T., Prototype laser-activated shape memory polymer foam device for embolic treatment of aneurysms. *J. Biomed. Opt.* **2007,** 12, (3), 030504.

129. Lin, J. R.; Chen, L. W., Study on shape-memory behavior of polyether-based polyurethanes. I. Influence of the hard-segment content. *J. Appl. Polym. Sci.* **1998,** 69, 1563-1574.

130. Glawe, J. D.; Hill, J. B.; Mills, D. K.; McShane, M. J., Influence of channel width on alignment of smooth muscle cells by high-aspect-ratio microfabricated elastomeric cell culture scaffolds. *J. Biomed. Mater. Res. Part A* **2005,** 75A, 106-114.

131. Andersson, A.; Olsson, P.; Lidberg, U.; Sutherland, D., The effects of continous and discontinous groove edges on cell shape and alignment. *Exp. Cell Res.* **2003,** 288, 177-188.

132. Curtis, A.; Riehle, M., Tissue engineering: the biophysical background. *Phys. Med. Biol.* **2001,** 46, R47-R65.

133. Flemming, R. G.; Murphy, C. J.; Abrams, G. A.; Goodman, S. L.; Nealey, P. F., Effects of synthetic micro- and nano-structured surfaces on cell behavior. *Biomaterials* **1999,** 20, 573-588.

134. Miller, D. C.; Thapa, A.; Haberstroh, K. M.; Webster, T. J., Endothelial and vascular smooth muscle cell function on poly(lactic-co-glycolic acid) with nano-structured surface features. *Biomaterials* **2004,** 25, (53-61).

135. Motlagh, D.; Hartman, T. J.; Desai, T. A.; Russell, B., Microfabricated grooves recapitulate neonatal myocyte connexin43 and N-cadherin expression and localization. *J. Biomed. Mater. Res. A* **2003,** 67A, 148-157.

136. Monkman, G. J., Advances in shape memory polymer actuation. *Mechatronics* **2000,** 10, 489-498.

137. Monkman, G. J., Controllable shape retention. *J. Intelligent Mater. Sys. Struct.* **1994,** 5, 567-575.

138. Tobushi, H.; Matsui, R.; Hayashi, S.; Shimada, D., The influence of shape-holding conditions on shape recovery of polyurethane-shape memory polymer foams. *Smart Mater. Struct* **2004,** 13, 881-887.

139. Tobushi, H.; Okumura, K.; Endo, M.; Hayashi, S., Thermomechanical properties of polyurethane-shape memory polymer foam. *J. Intelligent Mater. Sys. Struct.* **2001,** 12, 283-287.

140. Metcalfe, A.; Desfaits, A.; Salazkin, I.; Yahia, L.; Sokolowski, W.; Raymond, J., Cold hibernated elastic memory foams for endovascular interventions. *Biomaterials* **2003,** 24, 491-497.

141. Courtois, J.; Bystrom, E.; Irgum, K., Novel monolithic materials using poly(ethylene glycol) as porogen for protein separation. *Polymer* **2006,** 47, 2603-2611.

APPENDIX A

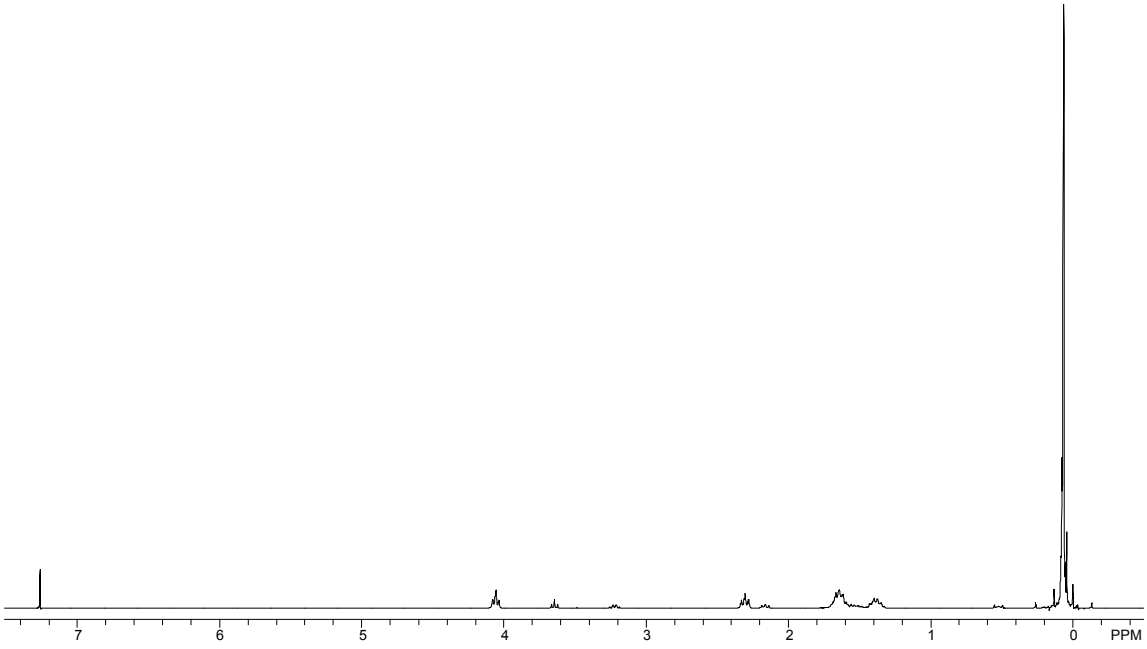

^{1}H NMR of HO-PCL$_5$-*block*-PDMS$_{37}$-*block*-PCL$_5$-OH (**a-P1**)

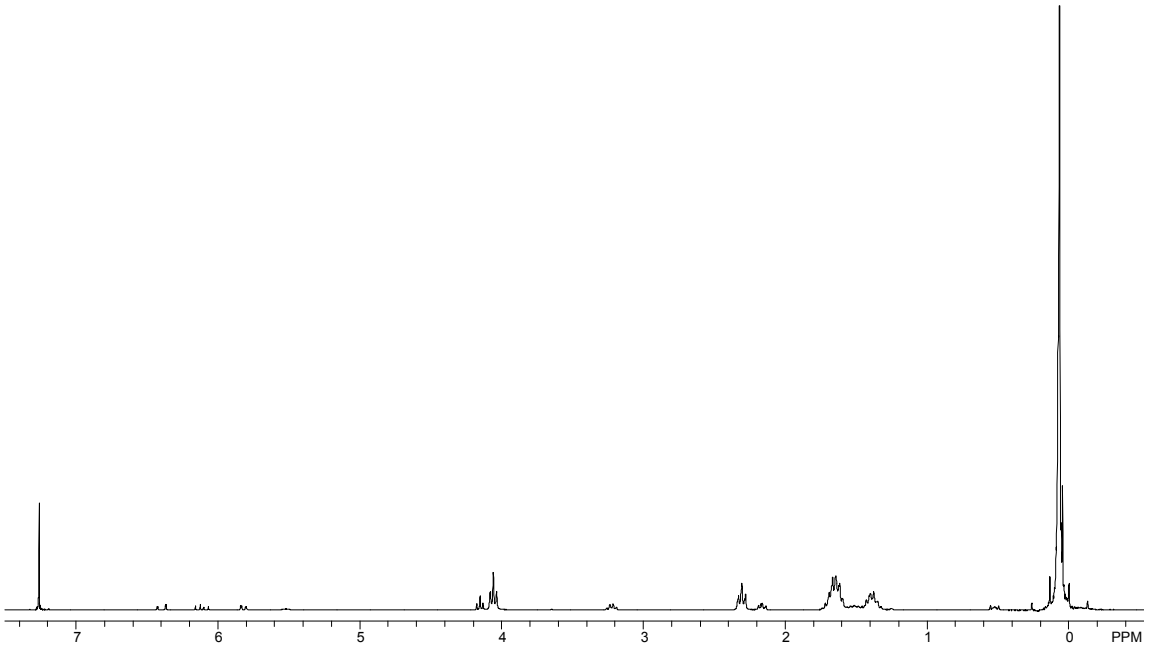

^{1}H NMR of AcO-PCL$_5$-*block*-PDMS$_{37}$-*block*-PCL$_5$-OAc (**b-P1**)

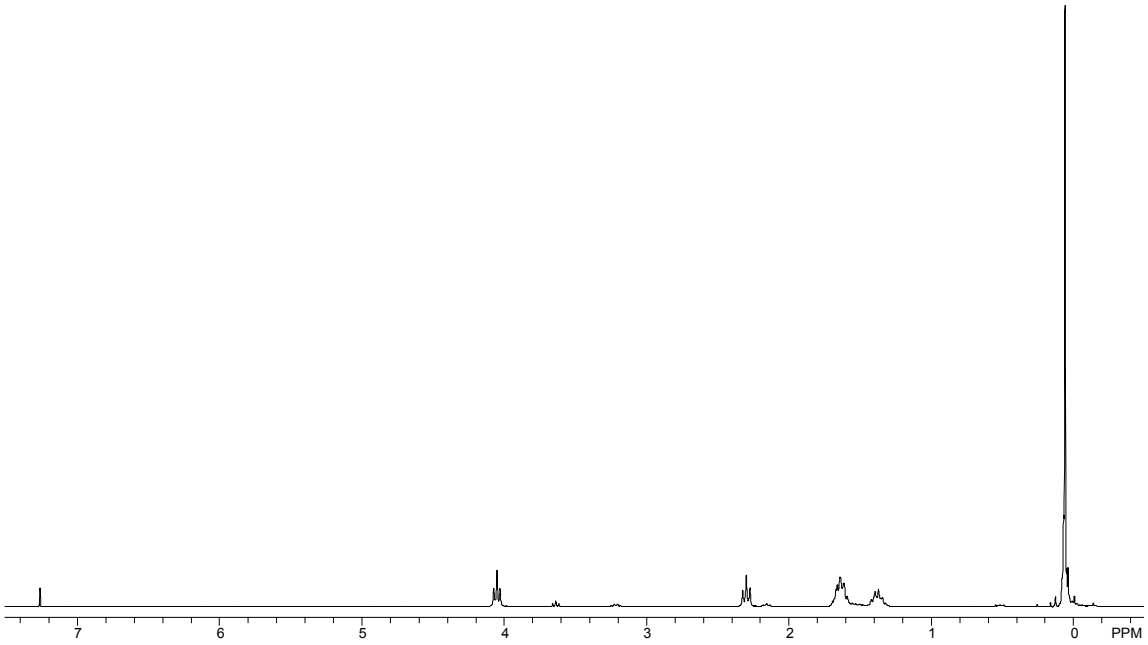

^{1}H NMR of HO-PCL$_{10}$-*block*-PDMS$_{37}$-*block*-PCL$_{10}$-OH (**a-P2**)

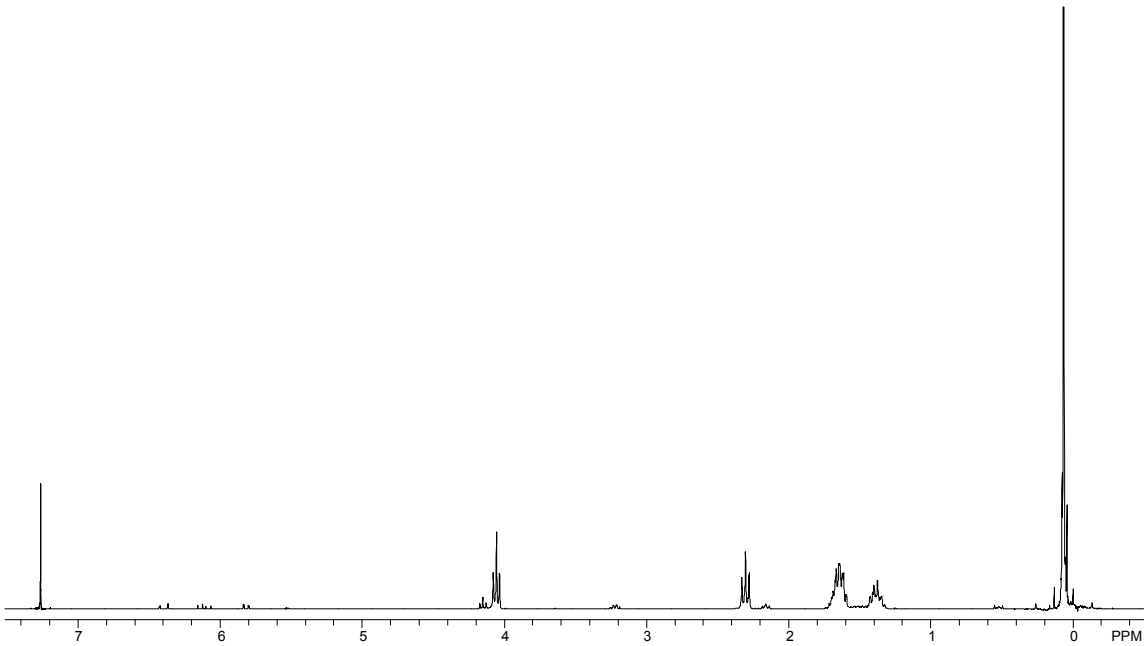

^{1}H NMR of AcO-PCL$_{10}$-*block*-PDMS$_{37}$-*block*-PCL$_{10}$-OAc (**b-P2**)

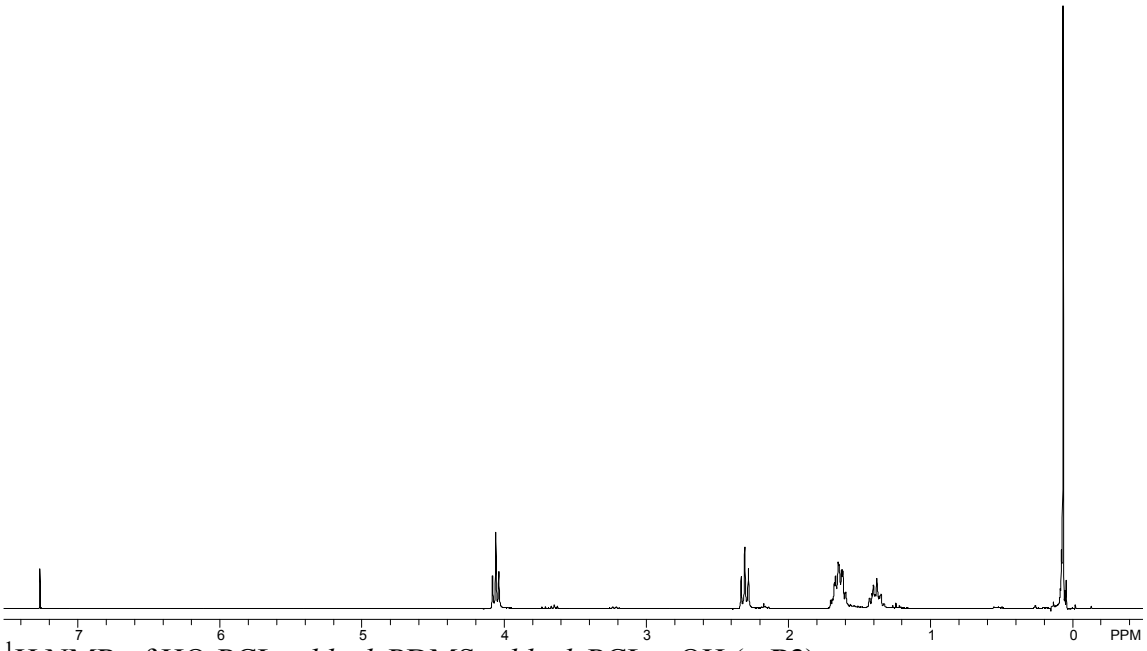

^{1}H NMR of HO-PCL$_{20}$-*block*-PDMS$_{37}$-*block*-PCL$_{20}$-OH (**a-P3**)

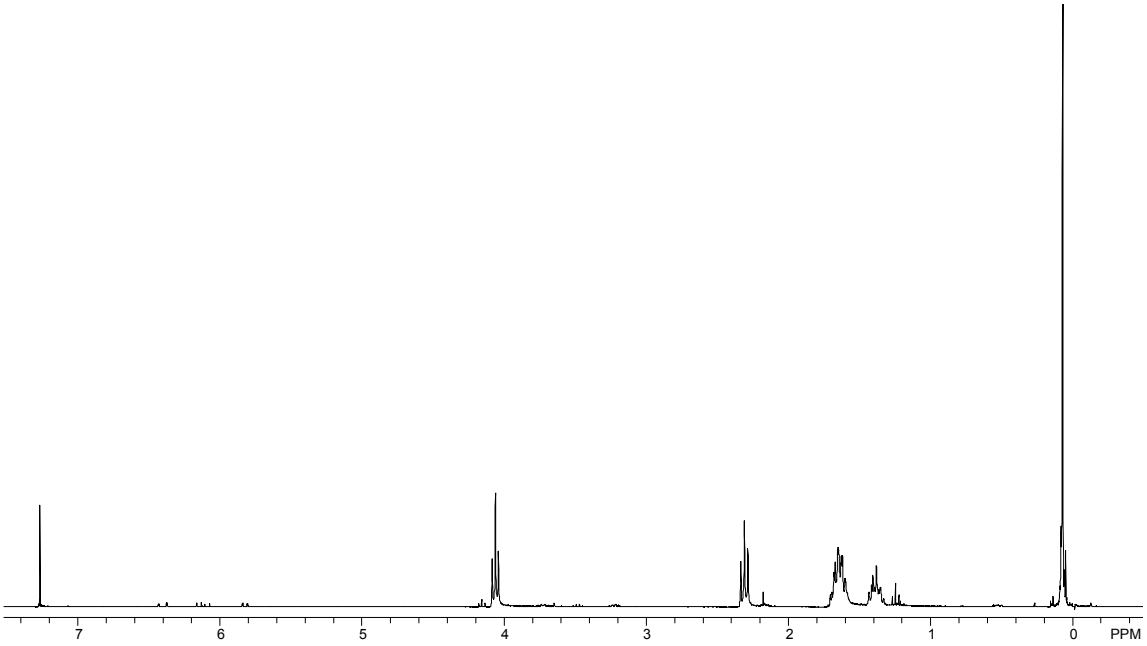

^{1}H NMR of AcO-PCL$_{20}$-*block*-PDMS$_{37}$-*block*-PCL$_{20}$-OAc (**b-P3**)

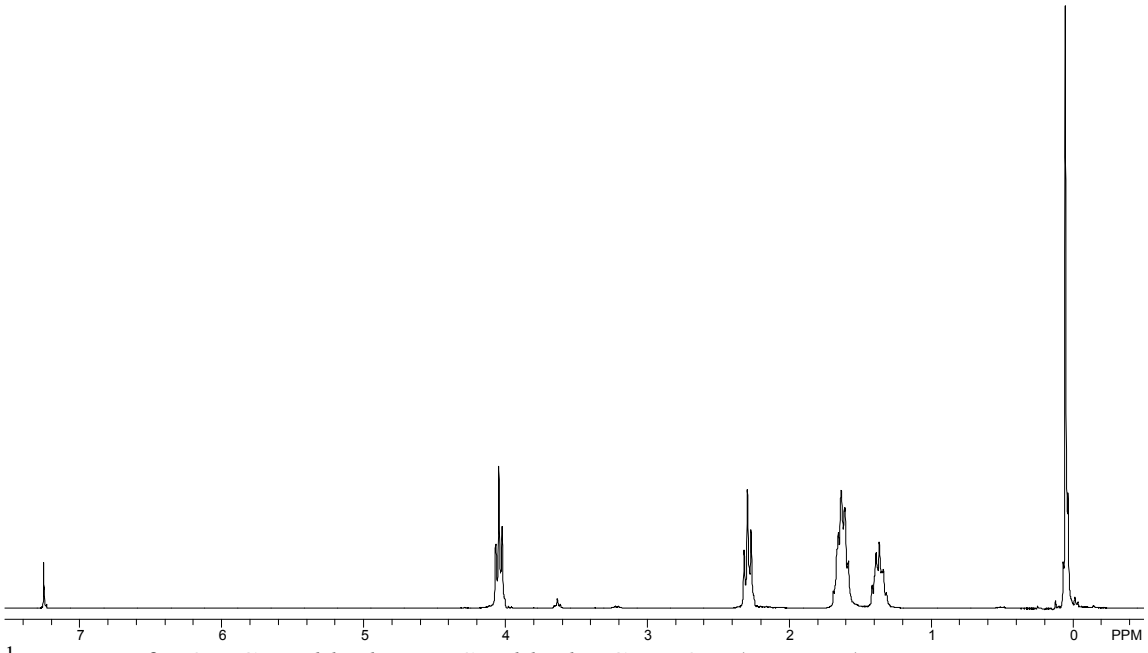

^{1}H NMR of HO-PCL$_{30}$-*block*-PDMS$_{37}$-*block*-PCL$_{30}$-OH (**a-SMP1**)

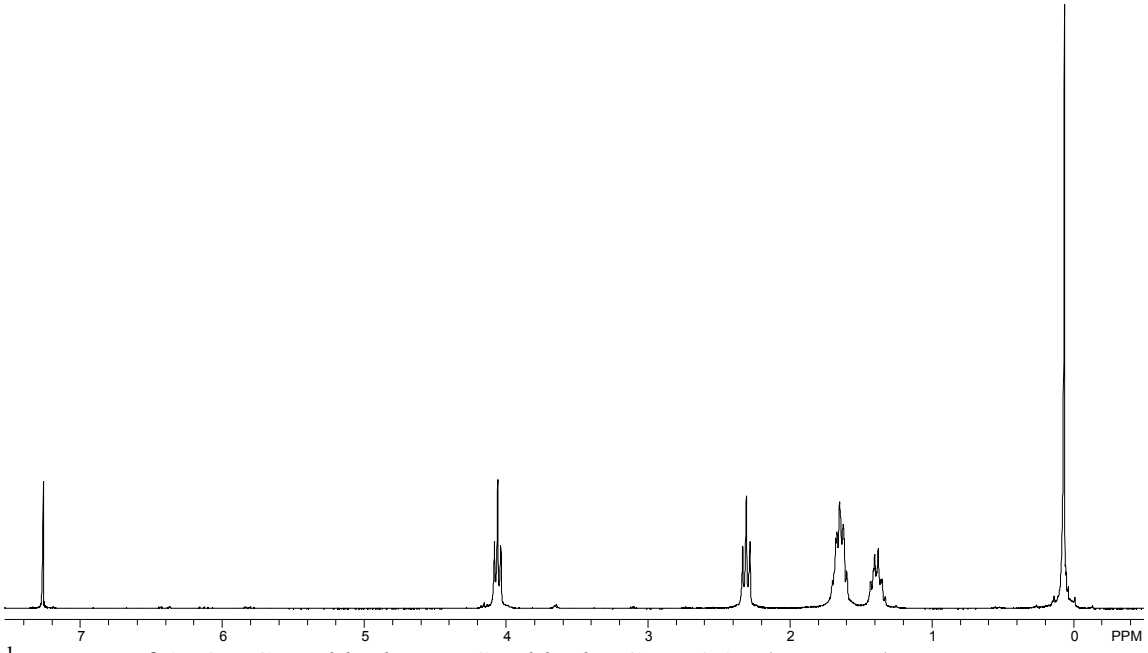

^{1}H NMR of AcO-PCL$_{30}$-*block*-PDMS$_{37}$-*block*-PCL$_{30}$-OAc (**b-SMP1**)

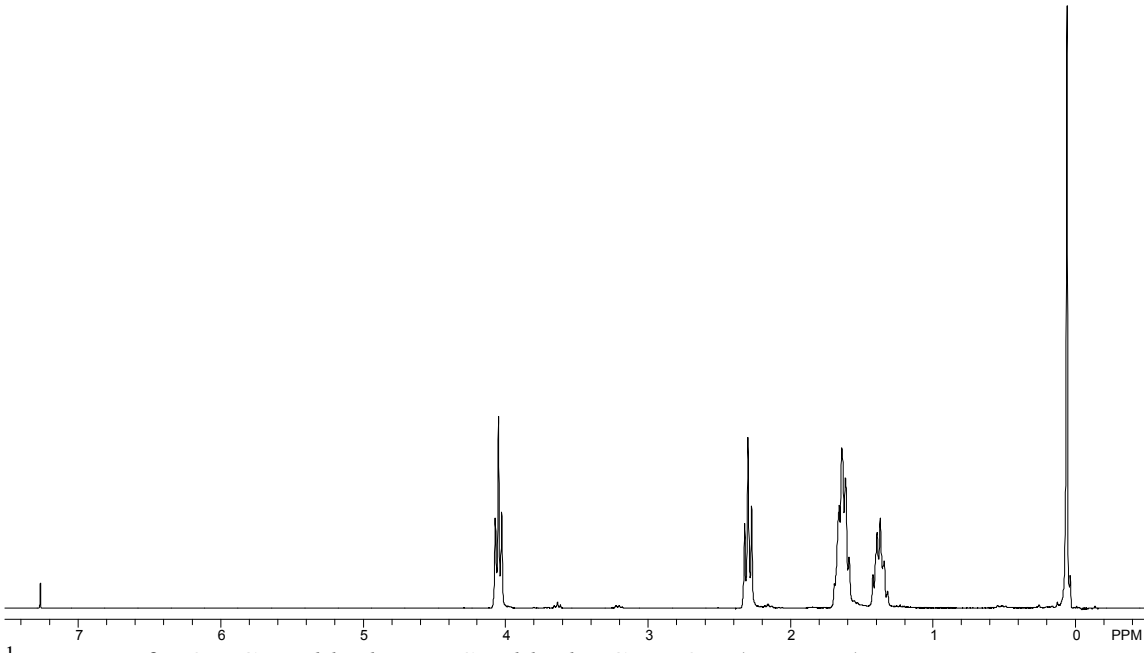

^{1}H NMR of HO-PCL$_{40}$-*block*-PDMS$_{37}$-*block*-PCL$_{40}$-OH (**a-SMP2**)

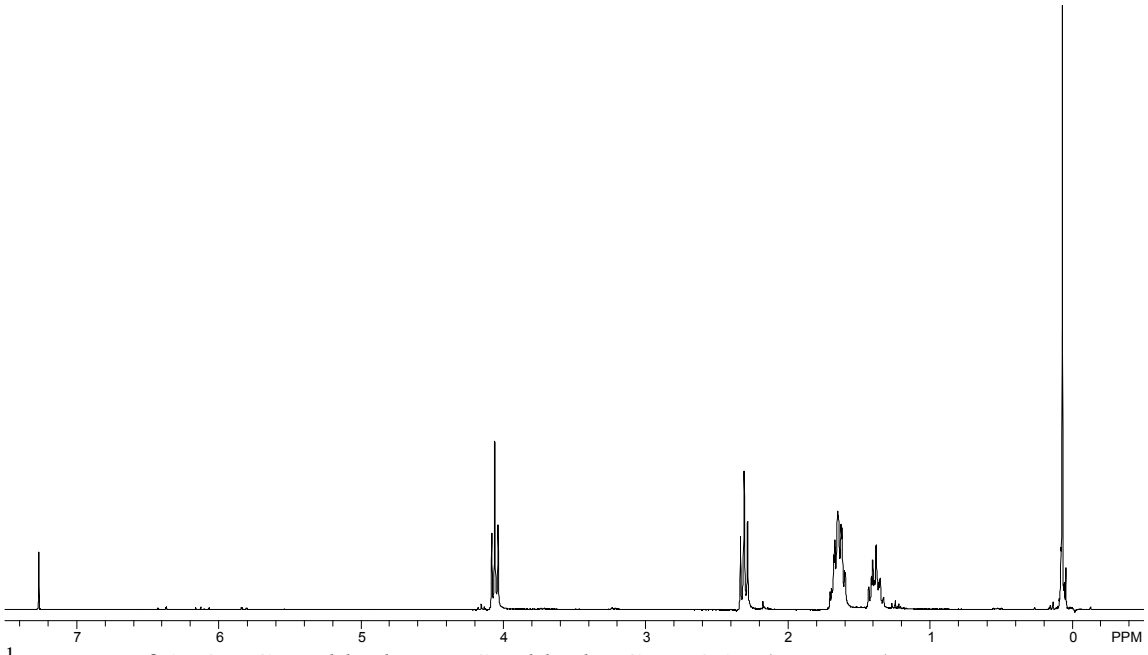

^{1}H NMR of AcO-PCL$_{40}$-*block*-PDMS$_{37}$-*block*-PCL$_{40}$-OAc (**b-SMP2**)

VITA

Cody A. Schoener received his Bachelor of Science degree in biomedical engineering from Texas A & M University, College Station, TX in 2007. He continued and received his Master of Science in August 2009 in the same department and institution as his B.S. His research interests include synthesis and characterization of novel Si-containing biomaterials for use in tissue engineering scaffolds or shape memory polymers. Expertise in mechanical, surface, thermal, shape memory, and microscopy techniques, including: (1) Nuclear Magnetic Resonance (NMR), (2) Fourier-Transform Infrared Spectroscopy (FTIR), (3) Gel Permeation Chromatography (GPC), (4) Thermal Gravimetric Analysis, (5) Dynamic Mechanical Analysis (DMA), (6) Differential Scanning Calorimetry (DSC), (7) Tensile Testing, (8) Goniometry/Contact Angle Analysis, (9) Environmental Scanning Electron Microscopy (ESEM), (10) Scanning Electron Microscopy (SEM), and (11) Field-Emission Scanning Electron Microscopy (FE-SEM).

Cody Schoener may be contacted through Prof. Melissa A. Grunlan at the Biomedical Engineering Department, Texas A & M University, College Station, TX 77843-3120.